

The Knuckleball Effect: How Design Variables Affect Aerodynamic Stability

A Major Qualifying Project
submitted to the Faculty of
WORCESTER POLYTECHNIC INSTITUTE
in partial fulfillment of the requirements for the
degree of Bachelor of Science

Prepared by:
Nora Smith
Elias Gonzalez
Noah Herzig
Tucker Carmichael

Thursday, April 25th, 2024

Report submitted to:
Professor Fiona Levey
Professor Aswin Gnanaskandan
Worcester Polytechnic Institute

This report represents the work of one or more WPI undergraduate students submitted to the faculty as evidence of completion of a degree requirement. WPI routinely publishes these reports on the web without editorial or peer review.

Abstract

The "knuckleball effect" in soccer, a random unpredictable movement of the ball when imparted little to no spin, which intrigues players, coaches, and fans with its unpredictability, results from variations in ball construction. Unlike other sports, soccer lacks standardized ball designs. This influences ball flight behavior significantly from game to game, especially when the ball is kicked with no spin. This project focused on understanding the knuckleball effect with two goals: reducing erratic movement by reducing lift forces and ensuring smoother airflow transitions. By analyzing created ball models, we aimed to create a stable design incorporating factors like seam length, panel symmetry, and surface characteristics. Through this research, we attempted to enhance soccer ball aerodynamics through a more consistent flight trajectory, particularly without rotation. Ultimately, our findings will inform the development of innovative designs aimed at minimizing the knuckleball effect, enhancing the quality and predictability of soccer ball flight in professional competitions.

Acknowledgements

The research team would like to thank the following people as without them, we wouldn't be able to conduct our research. Thank you to our advisors, Professor Fiona Levey and Professor Aswin Gnanaskandan for guiding us throughout this academic year and leading the team along the engineering process. Thank you to the WPI ARC lab for allowing us to use their facilities to conduct virtual wind tunnel simulation using ANSYS Fluent.

Table of Contents

This report represents the work of one or more WPI undergraduate students submitted to the faculty as evidence of completion of a degree requirement. WPI routinely publishes these reports on the web without editorial or peer review..... 1

Abstract.....	2
Acknowledgements.....	3
Table of Contents.....	4
Table of Figures.....	6
Introduction.....	8
Background.....	10
Design Constraints.....	15
Seam length and depth.....	16
Panel symmetry.....	16
Ball surface.....	17
Critical Reynolds number.....	17
Drag coefficient(s).....	18
Methodology.....	20
Virtual Simulations.....	20
Geometry.....	20
Meshing.....	23
Physics.....	24
Development Process.....	25
Limitations.....	26
Physical Testing.....	27
Wind Tunnel.....	27
Ball Launcher.....	28
Water Testing.....	29
Design Constraints.....	33
Simulation Data.....	34
Smooth Ball.....	34
Dimpled Ball.....	34
32 Paneled Balls.....	35
64 Paneled Balls.....	36
Model Comparisons - 60 mph.....	38
Model Comparisons - 80mph.....	40
Discussion.....	47
Wind Tunnel Simulations.....	47
Water Testing.....	50
Broader Impacts.....	52
Engineering Ethics.....	52
Societal and Environmental Impacts.....	52

Codes and Standards.....	53
Economic Factors.....	53
Conclusions.....	55
References.....	56
Appendix A: Unscaled Force Graphs.....	59
Appendix B: Force Difference Data.....	63

Table of Figures

Figure 1:	The first non-32 panel soccer ball for the FIFA World Cup, called TeamGeist	9
Figure 2:	The famous Jabulani official match ball known for knuckling in the FIFA World Cup	10
Figure 3:	The heavily researched Brazuca match ball used in the 2014 FIFA World Cup	10
Figure 4:	2018 FIFA World Cup ball Telstar 18	11
Figure 5:	2022 FIFA World Cup ball Al Rihla	11
Figure 6:	Nike's research lead to the development of a four panel ball with grooves to simulate dimples and longer seam length	12
Figure 7:	A F_L vs F_S graph for a used and new Telstar18 ball	13
Figure 8:	CAD of dimpled ball model	21
Figure 9:	CAD of smooth ball model	21
Figure 10:	CAD of 32 panel ball with deep seams	21
Figure 11:	CAD of 32 panel ball with shallow seams	21
Figure 12:	CAD of 64 panel ball with deep seams	22
Figure 13:	CAD of 64 panel ball with shallow seams	22
Figure 14:	General geometry setup of fluid body in Ansys DesignModeler	23
Figure 15:	General mesh setup of fluid body in Ansys Fluent, with flow direction highlighted	24
Figure 16:	Spool Calculations	31
Figure 17:	Diagram of the Pull Test	32
Figure 18:	The lift force vs flow time of the smooth ball model. All speeds are presented on one graph to convey the effect the change in speed has on the lift forces of the ball.	34
Figure 19:	The lift force vs flow time of the dimpled ball model at all speeds. Each simulation was only run for the amount of time needed to reach convergence, which is why the lines are different lengths.	35
Figure 20:	The lift force vs flow time of the 32 paneled ball with shallow seams model at all speeds. The y-axis scale was chosen for ease of comparison between all models, and thus not all wave patterns are visible.	36
Figure 21:	The lift force vs flow time of the 32 paneled ball with deep seams model at all speeds. This graph is scaled to the chosen y-axis, cutting off the information at the start of the flow behavior.	36
Figure 22:	Lift force vs flow time of the 32 paneled ball with deep seams model at all speeds, with the y-axis	37

	scaled to show force data at the beginning of the flow time.	
Figure 23:	The lift force vs flow time of the 64 paneled ball with shallow seams model at all speeds.	38
Figure 24:	The lift force vs flow time of the 64 paneled ball with deep seams model at all speeds. This graph is shown with the y-axis scaled for comparison.	38
Figure 25:	The lift force vs flow time of the 64 paneled ball with deep seams model at all speeds. This graph is shown with the y-axis scaled to visualize forces at earlier flow times.	39
Figure 26:	The lift force over a timeframe of 10 seconds of all models except the smooth ball at 60 mph. The timeframe used is 2-12 seconds of flow time, with the simulation setup portion taking place from 0-2 seconds. This corresponds to the 0-10 second timeframe used for the physical simulation analysis.	40
Figure 27:	The lift force over a timeframe of 10 seconds of all models at 60 mph.	40
Figure 28:	The drag force over a timeframe of 10 seconds of all models except the smooth ball at 60 mph.	41
Figure 29:	The drag force over a timeframe of 10 seconds of all models at 60 mph.	41
Figure 30:	The lift force of all models except the smooth ball at 80 mph over a timeframe of 10 seconds.	42
Figure 31:	The lift force of all models at 80 mph over a timeframe of 10 seconds.	42
Figure 32:	The drag force over a timeframe of 10 seconds of all models except the smooth ball at 80 mph.	43
Figure 33:	The drag force over a timeframe of 10 seconds of all models at 80 mph.	43
Figure 34:	32 Panel Deep Seam (8 mph)	44
Figure 35:	32 Panel Deep Seam (10 mph)	45
Figure 36:	32 Panel Shallow Seam (8 mph)	45
Figure 37:	32 Panel Shallow Seam (10 mph)	46
Figure 38:	72 Deep Seam (8 mph)	46
Figure 39:	72 Panel Deep Seam (10 mph)	47
Figure 40:	72 Shallow Seam (8 mph)	47
Figure 41:	72 Shallow Seam (10 mph)	48
Figure 42:	The physical representation of the lift force differences from time = 0s to time = 10s for all ball models at 60 mph. The data used to complete this graph was taken from the data points shown in Figure 26, and the table containing that data is located in Appendix B.	49
Figure 43:	The physical representation of the lift force differences from time = 0s to time = 10s for all ball models at 80 mph. The data used to complete this graph was taken from the data points shown in Figure 31, and the table containing that data is located in Appendix B.	50

Introduction

The purpose of this project was to investigate why the knuckleball effect occurs in the sport of soccer. The knuckleball effect occurs when a ball is kicked or thrown with very little to no rotation, resulting in the flight path being very erratic and unpredictable. Soccer does not have strict rules regarding how the ball should be constructed; the only regulated factors that official match soccer balls must meet are weight, circumference, limited water absorption, and shape retention. Other sports, such as baseball and basketball, have very specific rules for ball construction including number of stitches, required materials, and even mandatory colors. The lack of specificity in soccer ball construction results in many different manufacturers constructing various different soccer balls for different leagues around the world. These differences in construction lead to different number of panel numbers and shapes, ultimately affecting the way the soccer ball feels on the foot and flies through the air. The various soccer ball designs have different aerodynamics properties that can sometimes affect the outcome of a soccer game, due to the ball's possible unpredictable nature.

Goal(s):

Our ultimate purpose was to be able to design a soccer ball with a more predictable flight when there is no rotation. By having a ball design with a more consistent flight path, this will help showcase a player's talent and mitigate arbitrary outcomes within a soccer game. To do this, the goal of our research was to minimize the effects of the lift forces that produce the knuckleball effect in soccer. Two objectives were required to satisfy our goal: first, the transition between laminar to turbulent flow (or drag crisis) must occur at the lowest possible Reynolds number to

maximize ball stability; second, the lift within a side force (F_s) vs. lift force (F_L) graph must produce forces as close to zero newtons as possible.

Expectations:

Within the given timeframe, the team hoped to accomplish the following: 1) Gather data from ball models that encompass the primary design elements of soccer balls 2) Test and gather data from new ball designs 3) Finalize the design of the stable ball model 4) File for a patent and 5) Talk to a WPI intellectual Property Lawyers and manufacturers about constructing our design. We were very hopeful that all five aspects mentioned above would be completed. Despite a few points during our research where we came to an obstacle or roadblock, we defined this project as a “success” since we were able to at least accomplish the second task.

Since we were not able to have a physical model of our ball, produce a CAD file, or establish a patent, there are a few ways for the project to continue after the completion of the MQP capstone. Development of a model and additional testing would be required, along with revision and retesting. Afterwards there are two main courses of action: 1) Crowd fund and start a company or 2) Sell the design to another company for them to produce.

Background

The most popular sport in the world is soccer, this past FIFA World Cup tournament had 1.5 billion viewers throughout the world (1). With many teams and fans sharing the passion for the game, people take the World Cup seriously because it is the most prestigious level of play. Recently fans and players alike have become frustrated with the most important piece of equipment, the match ball. Unlike other sports, soccer doesn't have defined rules as to how the ball shall be constructed; for example, baseballs are required to be two white panels made from genuine cow leather, have a yarn wrapped cork core, a circumference of 9.25", and a weight of 5.25 oz (2). In the NFL, the ball must be specific in its dimensioning, weight, color, set of materials, and must be provided by the company Wilson (3). Unlike those sports, soccer is relaxed in the sense that the ball's design can be delegated to the company's interpretation. The broad rules regarding the ball leave the design and manufacturing up to the ball providers for each given league and tournament. Interpretations of the design will vary drastically from each company, but the inconsistent construction also changes the aerodynamics of each ball. By not standardizing ball design used in professional games, players are forced to adjust to different ball behaviors in a short time. This was an issue especially during the last few World Cups. Since the World Cup started in 1930, the host nation would provide the soccer ball for the competition. In 1970, Adidas became the ball manufacturer for the World Cup and remains today (29). Since Adidas became the ball provider, they have constructed a 32 panel soccer ball and have been using the same design until 2002, despite making minor changes such as changing the panel cover material from genuine leather to a synthetic leather. By keeping the 32 panel design, it ensured consistency throughout the entire 90 minutes of play between years of competition. In

2006, as shown in figure 1, Adidas changed the ball construction to 14 panels and made it thermally bonded rather than hand stitched, resulting in the ball flying unpredictably at times and causing many complaints (30).



Figure 1: The first non-32 panel soccer ball for the FIFA World Cup, called TeamGeist (33)

In 2010, Adidas made another design change, as shown in figure 2, this time an 8 panel ball was manufactured claiming it (31) was more aerodynamically stable than any other ball in the past. This statement wasn't true (30) and instead was erratic in flight similar to the previous 2006 World Cup ball. Players and fans complained (30), comparing it to a beach ball as well as calling it a disgrace to the sport because the most simple and important piece of equipment couldn't be made correctly. This led to a number of missed scoring opportunities and lucky goals (5), ultimately making the ball being the deciding factor of which team will win despite the teams' exceptional talent.



Figure 2: The famous Jabulani official match ball known for knuckling in the FIFA World Cup (34)

In 2014, as shown in figure 3, Adidas revealed once again a new ball for the tournament, which was a 6 panel ball. This time Adidas spent some time making another ball design claiming that it had better stability and as a result added micro dimples, increased seam length, and made the seams deeper (28).



Figure 3: The heavily researched Brazuca match ball used in the 2014 FIFA World Cup (33)

The last two World Cups, 2018 and 2022, the soccer balls have been more stable in flight (27) but continue to differ in how they fly and feel because once again Adidas changes the design every competition, as shown in figures 4 and 5.



Figure 4 & 5: (Left) 2018 FIFA World Cup ball Telstar 18 (33), (Right) 2022 FIFA World Cup ball Al Rihla (35)

This isn't an issue in just the World Cup, other leagues around the world have different ball providers who construct the ball differently and as a result players and fans don't get consistency within each game. With a lack of consistency in terms of panel design of a soccer ball, at high levels of competition players are sometimes unable to showcase their skill and hard work due to the ball affecting the outcome of the game. Developing a more predictable ball has been a focus of many ball manufacturers in recent years, resulting in companies such as Nike to introduce Aerotrack Grooves (26), which are indents on the panels to simulate a longer seam length, as shown in figure 6.



Figure 6: Nike's research lead to the development of a four panel ball with grooves to simulate dimples and longer seam length (36)

The study of the aerodynamics of soccer balls is a relatively recent undertaking, but some general data has been found through research. The flow of air around the ball can be looked at using fluid mechanics; once the critical Reynolds number (Re_{crit}) is reached at a certain speed, the airflow around the ball begins to shift from laminar to turbulent. This is known as the critical period. During this period, the drag coefficient (C_D) drops considerably. As Re_{crit} continues to increase, eventually the flow becomes fully turbulent. Once this happens, the flow enters the supercritical phase. C_D begins rising again, albeit much more slowly, and the Re_{crit} range ends. The Re_{crit} range for existing ball patterns has been observed to begin between $Re = 2.2 \times 10^5$ and $Re = 3.0 \times 10^5$ (7). Additionally, the transition speeds of existing soccer ball designs ranged from 5.5 to 9.5 m/s at the onset of turbulence, and 13.5 - 21 m/s as turbulence ended (8). While the behavior of the ball is consistent during the supercritical phase due to the even lift and lateral forces, there is asymmetry present in the critical phase that causes unpredictable movement.

Mapping the lift force coefficient (C_L) and the lateral force coefficient (C_S) of a ball onto a graph such as Figure 7 shows its tendency to swerve.

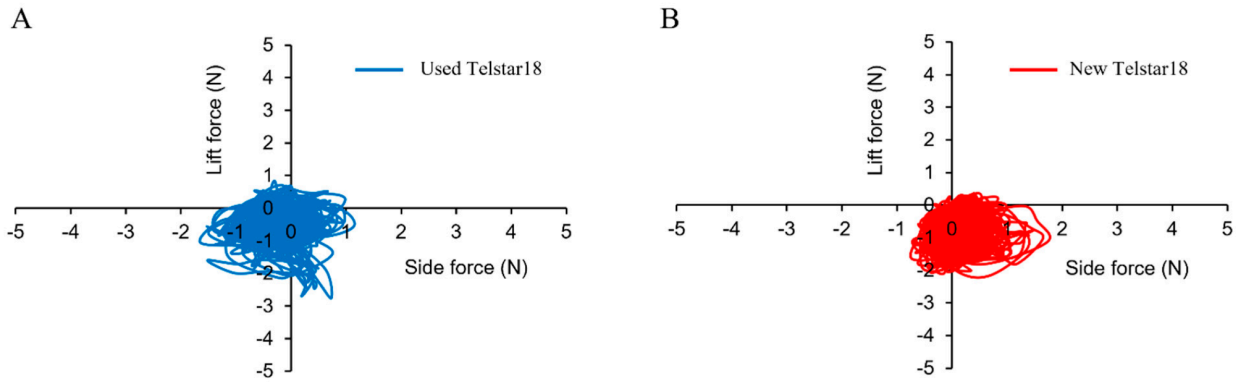


Figure 7: A F_L vs F_S graph for a used and new Telstar18 ball. (19)

This swerving and irregular ball behavior is known as the knuckleball effect. The knuckleball effect occurs when a spherical ball is thrown or kicked in such a way that there is very little to no spin. It has been observed that the geometry of soccer balls creates stable flight when kicked with spin, but less predictable patterns of movement when kicked without spin (6). This compounds the game impact that the knuckleball effect has, making soccer balls with a tendency to knuckle more difficult to shoot accurately.

Design Constraints

When evaluating the behavior of a soccer ball, a number of design elements come into play. From those existing elements, the variables that we deemed the most important to test were selected: seam length and depth, surface smoothness, and panel symmetry. Additionally, ball behaviors were broken down to the two most important non-dimensional variables: the critical Reynolds number and the drag coefficients. While most papers focus on ball behavior as it relates to spin or ball orientation, there is some existing data that compares various ball

constructions. Note that the effects of spin were often not isolated from the potential impacts of design changes.

Seam length and depth

It has been shown through wind tunnel testing that when a soccer ball is spinning, the seams serve to stabilize its flight (6). However, long seams perpendicular to the flow direction have been noticed to increase drag forces on the ball, which contributes to additional curve (6). This is a problem for balls kicked with no spin. Designs with longer seams are also observed to have larger C_D differences in different ball orientations, making consistency more difficult (12). Seam volume is also important, and involves both seam length and seam depth. Ball designs with more seam volume had lower Reynolds numbers for the beginning and ending of their drag crises. Additionally, balls with higher seam volume remain in the supercritical region longer, keeping the changes in flow conditions small and resulting in more stable flight (8). However, designs with deeper seams show a larger increase of C_D over time as the Reynolds number continues to increase, contributing to more unpredictable behavior at higher speeds and over longer kicks (12).

Panel symmetry

While the number of panels is often the most noticeable thing about a ball design, it does not contribute much to aerodynamic behavior on its own. Rather, panel number is related to seam volume, as more panels means more seams. Additionally, the configuration of panels can create longer seams, which increases drag forces as previously stated. Configuration of panels also affects ball symmetry: when a ball has an asymmetrical pattern, lift forces show greater

unbalance between axes than symmetrical balls. These asymmetrical forces contribute to unpredictable behavior in a non-spinning ball (9).

Ball surface

Dimpling effects on panels have also been studied. Rougher surfaces have been noticed to cause flow transition at lower flow speeds and at lower Reynolds numbers (8). This has been tested through a study using five soccer ball models with different forms of ball texturing, all with the same 32 panel design (22). This study gathered data and noticed that for almost every other ball texturing, except for dimpling, there were uneven side and lift forces (22). Their conclusions were that a soccer ball with their specific dimple setup will have side and lift forces that are almost identical (22). Aside from physical characteristics, general ball behavior as well as the knuckling effect can be observed and recorded mathematically through the definitions of the non-dimensional variables.

Critical Reynolds number

The critical Reynolds number of a system is the point at which flow behavior changes from laminar to turbulent. Often, this will not be a singular value but a range of numbers. The equation we will be using to determine the Reynolds number of a system is:

$$\text{Re} = \frac{uL}{\nu}$$

where u = flow speed, L = characteristic length, and ν = kinematic viscosity. Since we will be testing spherical balls, our characteristic length will be the diameter of our models. The only medium tested will be air, so our kinematic viscosity will be defined by the temperature of the air used. Finally, flow speed will be the variable used to determine how different design choices affect the critical Reynolds number.

Drag coefficient(s)

The drag coefficient of an object is a quantification of the resistance of an object's movement through a fluid. Its representative equation is such:

$$c_d = \frac{2F_d}{\rho u^2 A}$$

where F_d = the force in the direction of flow velocity, ρ = density of the fluid, u = flow speed, and A = reference area of the object. Since the curve behavior of a ball is dependent on the forces acting upon it, this equation will be important when looking at flight behavior. The drag coefficient equation can also be applied to the other axes of motion; namely, lift as C_L and lateral as C_S . All of these variables were examined in order to most accurately predict the occurrences of the knuckling effect. Since the knuckling effect is observed with the occurrence of the drag crisis, the timing of which varies depending on ball design, our design goal is to induce the knuckling effect early so that ball behavior remains consistent at higher speeds. This will be done through controlling the non-dimensional variables through specific design elements.

Outside of the ideal non-dimensional variables, any designs created need to be compliant with existing regulation for match balls. The circumference must be between 68 and 70cm, the weight must be between 410 and 450 grams, the overall shape of the ball must be a sphere made from an approved material, and the initial pressure of the ball must be between 0.6 and 1.1 atm (4). Additionally, we considered what costs will be involved in the project process. These costs included the manufacturing and materials used to create models, manufacturing costs for a final design, and the patent application fee should we get that far. Depending on the nature of the design testing, costs could have included equipment rental or laboratory access somewhere other than WPI.

Our research goals included learning the effects of seam depth and dimpling on the non-dimensional variables, as well as confirming the effects of seam length and panel number. This knowledge will then be applied to our own designs in order to meet our overall project goal.

Methodology

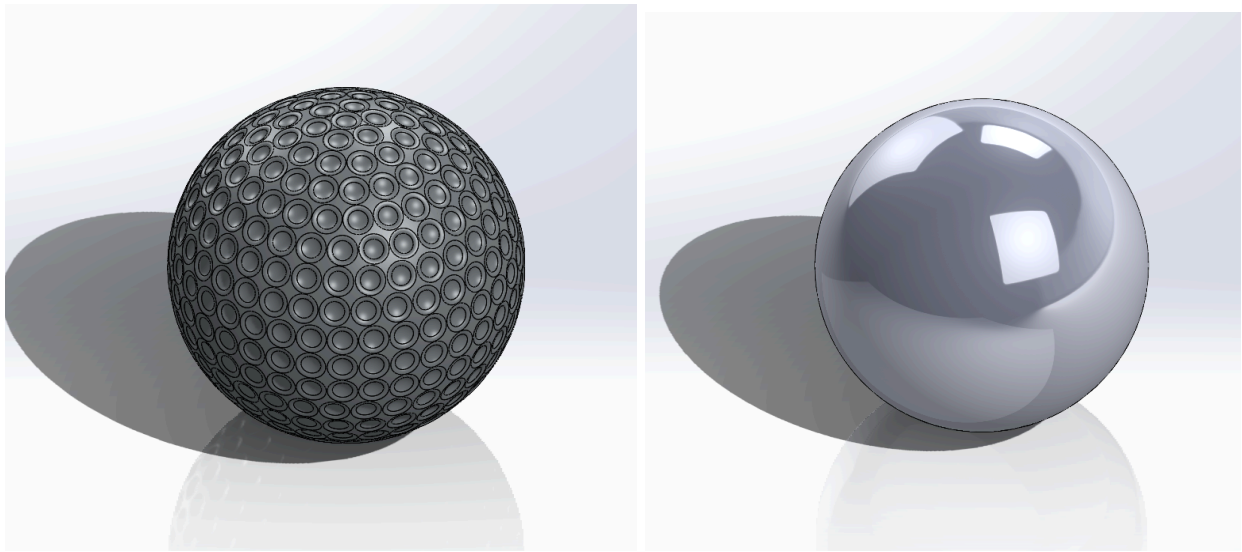
Virtual Simulations

In order to determine the effects that each design element has on the relationship between the Reynolds number and external forces, as well as the onset of turbulence, Computational Fluid Dynamics (CFD) simulations were used. These simulations had two main goals: to quantitatively compare force differences between the models, and to form hypotheses around the physical testing results using that data. The simulation software used was the 2023 version of ANSYS Fluent to meet industry standard. The general simulation methodology is adapted from chapter 5 of Computational Fluid Dynamics for Sport Simulation, by Sarah Barber and Matt Carré (6).

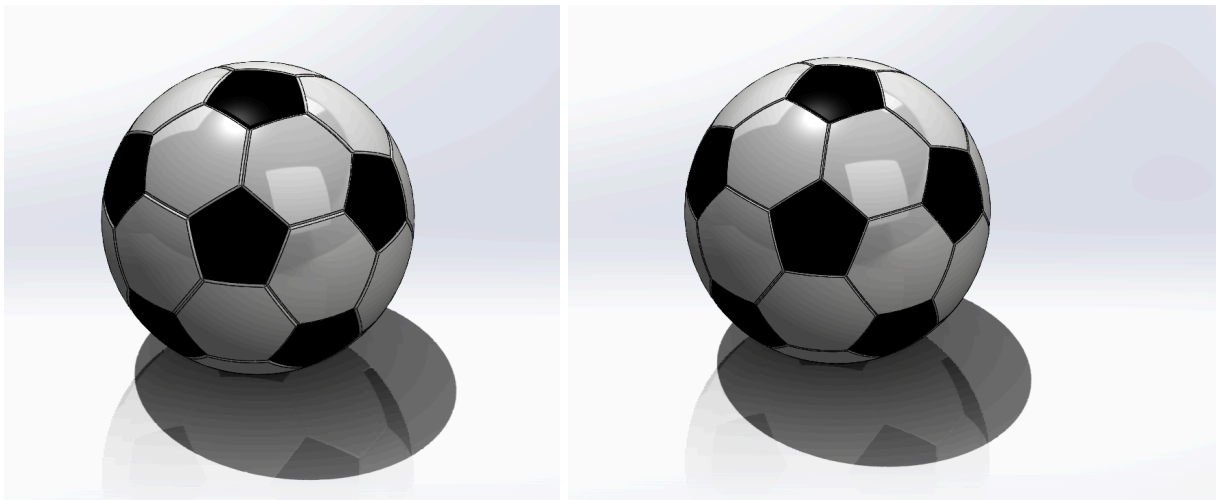
Geometry

In order to reduce rendering times and avoid potential complications with 3-dimensional meshing, our project focused primarily on 2-dimensional simulations. However, to ensure model accuracy, the initial models were made in 3D using Solidworks to accurately capture the geometry of each ball. The three major design elements of a soccer ball were isolated in each model: panel symmetry, seam depth, and ball texture. Two base models were used to test panel symmetry: the first design had 32 panels (seen in Figures 10, 11), while the second design had 64 (seen in Figures 12, 13). These differing panel numbers were created by extending the lengths of the seams to create more panel divisions. Additionally, two seam depths were tested for each model. The shallow seam depth was 1.10 mm, while the deep seam depth was 1.7 mm. For ball texture, a dimpled ball model reminiscent of a golf ball was created (seen in Figure 8), with a dimple depth of 3 mm. Finally, a smooth ball was modeled to serve as our control for the simulation setup, shown in Figure 9.

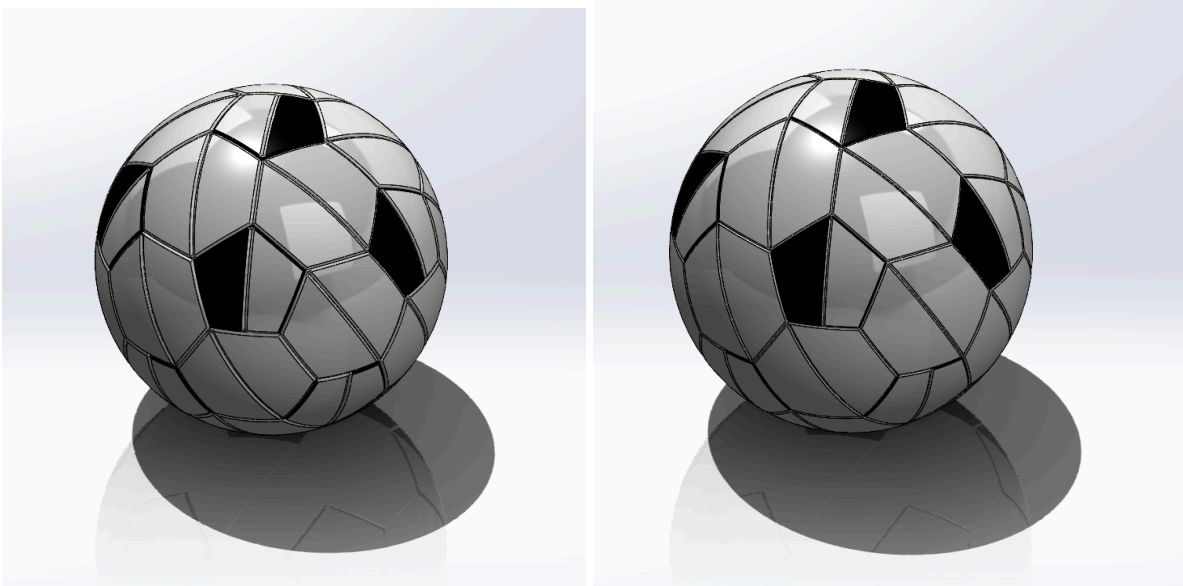
These seam depths were gathered by averaging the best performing depths, in terms of earliest transition and average lowest drag coefficient (13-19). In order to decide on the dimple depths, previously researched golf ball designs were analyzed to see which had the least amount of drag, and which had the earliest transition from laminar to turbulent flow due to the drag forces (10, 11).



Figures 8 & 9: (Left) CAD of dimpled ball model, (Right) CAD of smooth ball model



Figures 10 & 11: (Left) CAD of 32 panel ball with deep seams, (Right) CAD of 32 panel ball with shallow seams



Figures 12 & 13: (Left) CAD of 64 panel ball with deep seams, (Right) CAD of 64 panel ball with shallow seams

In order to convert the 3D models into 2 dimensions, a cross-section of each model was created by creating a slice through the middle. This preserved both the radius of the model as well as the important geometric features. After each model's cross-section was created and saved separately, the new geometry was imported to ANSYS Workbench. Workbench was used in order to better manage the geometry, mesh, and simulation files for each model. Once the ball geometry was imported and adjusted to sit on the 2D plane, the fluid area was created. A surface area of 7.5 m by 5 m was used to minimize potential flow issues. These dimensions also create a cross-sectional ratio of about 10:1 between the fluid and the ball model, similar to the ideal ratio in a wind tunnel. For simplicity of setup, the "modeling ball" was created by subtracting the ball geometry from the fluid geometry to define the different regions more easily. The result of this process is shown in Figure 14.

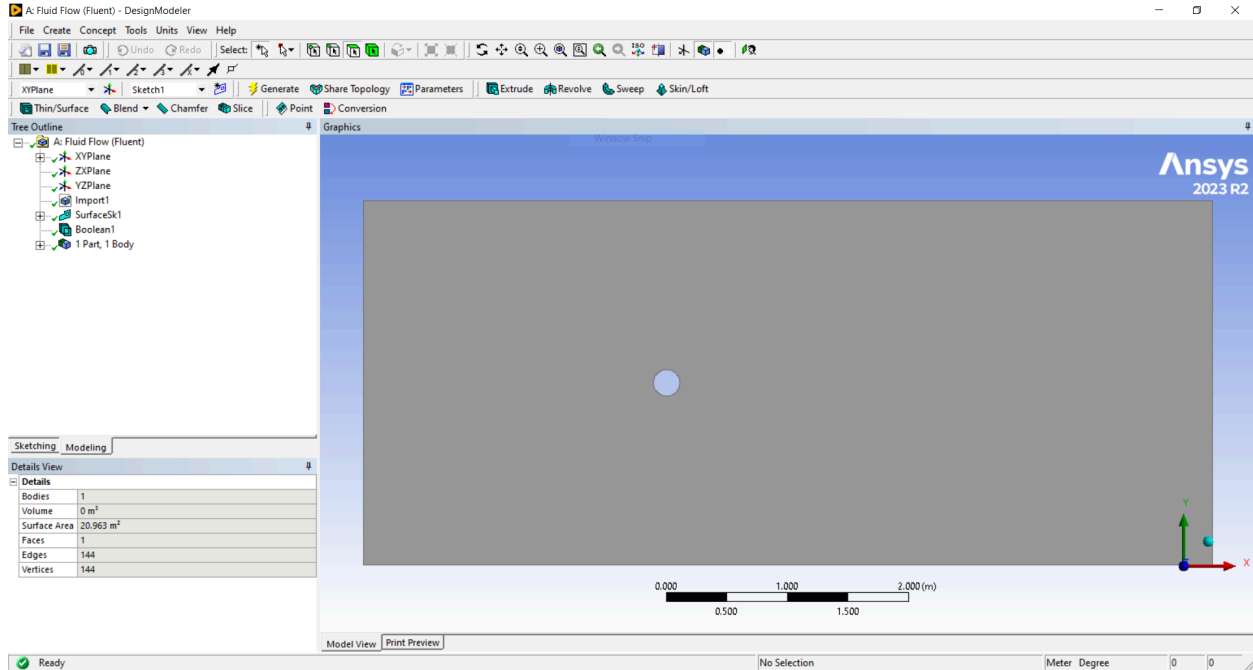


Figure 14: General geometry setup of fluid body in Ansys DesignModeler

Meshing

Each fluid mesh was created following the same general process, with differences in resolution depending on the features being tested. All meshes were constructed using the triangles only method, with a quadratic element order to follow the shape of the ball more closely and increase the resolution at the edge of the ball model. Capture curvature was enabled, while all other settings remained on their default values. The element size was typically 0.15 m, but the default element size was used when necessary, as smaller element sizes tended to cause geometry issues with the seams. An inflation was added to increase the resolution in the area of interest. The ball edges were defined as the boundary, and a first layer height of 1×10^{-7} m was used. The inflation growth rate remained at 1.2, the default value. The maximum layers varied from 45-60 depending on the shape the inflation took as it expanded outward. Since the desired data was related to turbulence and drag forces, there was no need for the majority of the fluid

region to have a high resolution, although the general setup led to a wake region with enough definition to make out general behavior. Finally, all sections of interest in the mesh were identified prior to beginning the physics setup. These selections consisted of the velocity inlet, pressure outlet, wall (defining the ball), no-shear boundaries and fluid body. The final mesh, as seen in Ansys Fluent, is pictured in Figure 15.

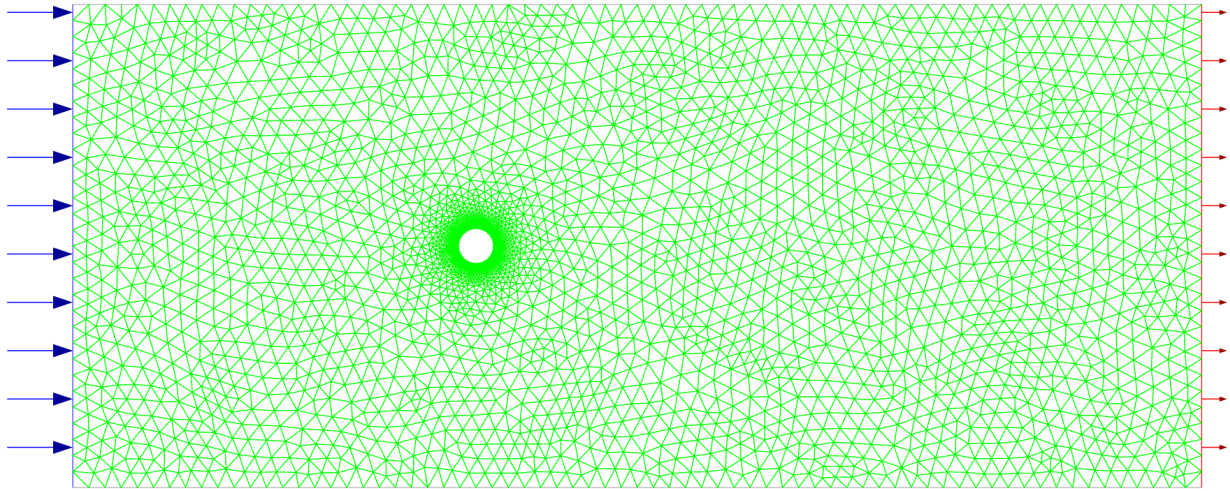


Figure 15: General mesh setup of fluid body in Ansys Fluent, with flow direction highlighted

Physics

Barber and Carré's model (6) used the $k-\omega$ SST turbulence model, which includes two additional transport equations in order to define the turbulent flow properties. These models were used in circumstances where mean pressure gradients were small, making it an applicable model for wind tunnel-esque simulation (24). A second-order upwind scheme was used for the velocity discretization. This scheme allows for greater accuracy within the space by creating a Taylor expansion at each cell face (25). A corner correction was also applied in order to get more accurate data, since the models had sharper edges along each geometry element.

General restrictions used by this technique include that there is no refined wake region and the ball surface is defined as a no-slip wall. Additionally, the inlet is defined by the fluid

velocity and the outlet is specified as a pressure outflow. These conditions were found to be comparable to wind tunnel visualizations, and thus allow for the simulation to be used to compare the aerodynamics of different ball designs.

Default values for air were applied to the fluid body. Since gravity was not applicable, and the material was not a considered variable, the material properties of polyurethane (the typical coating of soccer balls) were applied to the ball wall. A transient setup was used to track the development of flow patterns. The speed used for each test was applied to the inlet condition (defined previously, in the meshing stage). For calculations, a timestep of 0.15 seconds was used. This timestep was chosen to balance computing time and detailed wave patterns. 60 iterations per timestep were used for the same reason. Finally, the simulation ran for 1800 timesteps, which allowed for complete development of flow behavior in most cases. If the simulation reached convergence before then, Ansys Fluent stopped calculations without additional input. Data collection was done through two force reports: one for the drag force over time, and one for the lift force over time. These reports collected the force data at each timestep and created graphs. Visually, the flow behavior of each ball was modeled through Fluent's in-program animation process. This was done through the creation of velocity vectors applied to the fluid body. Animation allowed for the visualization of turbulence, as well as any wave patterns caused by the knuckleball effect.

Development Process

In order to create simulations where data could be compared quantitatively, simulation setup needed to be internally consistent. Even if the goals were not to generate "true to life" data, all data needed to be accurate within the scope of the project. This was done through trial and error, and validated by the results of both control models. While much of the geometry

development was straightforward, a technique needed to be developed to convert the most symmetrical slice along the y-z plane to the x-y plane for simulations. The meshing software had a slight learning curve, but once an element size that caused no interfacing issues was found, most issues resolved themselves. Most of the experimentation happened during the physics setup. The control models had known behavior that needed to be produced before moving forward into the more unknown geometries. Since there are so many different ways to set up a simulation in Fluent, it was difficult to identify where exactly any issues were coming from. Despite this, having two controls allowed comparisons to be made right off the bat. This meant that as soon as one setup worked for both controls, it could be used for the rest of the models. This ensured that all data comparisons were able to be accurately compared, and therefore able to be applied to physical testing qualitatively.

Limitations

Highly asymmetrical ball designs, similar to baseballs and cricket balls, were not tested as these designs are highly reliant on orientation. Additionally, it is already known that they will produce asymmetrical lift forces if they were to be in flight without spin (19, 20). The lack of detailed wake formation means that visualizing the exact knuckleball behavior will not be possible. However, the primary focus is the forces, so the wake region is not a major concern. Finally, the models themselves were not designed to be used in 2D, which created some interfacing issues during mesh generation. While meshing decisions were made to work around that, it is possible that small errors still affected the force data.

Physical Testing

In order to corroborate the results from the simulations, the group also physically tested the designs to visualize the ball path through air during the knuckling event. The simulations provided data that enabled the group to focus testing efforts into a smaller range by showing the Reynold's number when the ball is expected to reach its drag crisis.

The Reynold's number range from the initial calculations is 335005 to 764713 which is about 40 mph to 80 mph for a 9" diameter round object in air. Our options for physically testing the designs included: wind tunnel testing, developing a ball launcher, and water testing

Wind Tunnel

Our first choice for physical testing was using one of the multiple wind tunnels available on the WPI campus. The group would create 3D-printed models scaled down to size and mount them to a three-axis force sensor within the wind tunnel. The three-axis force sensor would allow the group to measure the force on the lateral and vertical forces on the ball throughout a range of speeds. The force sensors would allow the team to identify the change of flow from laminar to turbulent. The speed at which this flow change occurs The wind speeds for the scale model would be calculated to match the Reynold's number range determined in the simulations. As the wind speeds increase, the forces on the ball should constantly increase, and if the wind speed is constant, the forces on the ball should remain constant. The speed, or range of speeds, at which the ball has erratic forces, is the point of its drag crisis. These speeds are then used to calculate the Reynold's number. The Reynold's number found in testing would then be used to determine what air speed a full size soccer ball would experience it at.

There are three separate wind tunnels available on the WPI campus which include the aerospace departments, mechanical departments, and the Fire Protection department. The main

constraint with each of the wind tunnels is the size of the model that would be able to fit in each tunnel as well as the maximum speed that can be used in said tunnel. As the ball is scaled down the wind speed must go up to produce the same results as a full scale soccer ball. Therefore only one tunnel was able to give proper results and that was the aerospace tunnel. Each model can occupy a maximum of 10% of a wind tunnel's cross sectional area. The mechanical department's tunnel has a cross sectional area of 6" ft by 6" the maximum size ball we would be able to put in this tunnel would be about 1.2 inches in diameter, which is 7.5 times smaller than a normal ball. At this ratio a similarity in Reynolds number for 80 mph would be achieved at a wind tunnel speed of 600 mph. This tunnel was designed for low speed and low turbulence and would not be able to support these speeds, and therefore it was not a viable option. In addition to this the mach number of 600 mph is 0.78, much greater than 0.3, the upper limit of testing validity. The Fire Protection wind tunnel was also not an option due to the wind speeds. The tunnel itself is very large and would be able to fit a ball twice the size of a normal ball, the issue with this tunnel is that it was made to simulate mountain winds to exhibit fire spreading in a forest. These wind speeds only reach 5-6 mph which is too slow for a model twice the size of a normal soccer ball, so we ruled this wind tunnel out. The only wind tunnel that had the proper size and wind speeds was the aerospace department's wind tunnel. Despite the usefulness of the facility, our team was denied access to it which is why we began exploring different opportunities to discover the transition speed required to compare the design variables.

Ball Launcher

The second choice for physical testing was developing a ball launcher to propel the 3D models and use two high speed cameras, one positioned directly behind the launcher to track the side to side movement of the ball. The other positioned perpendicular to the launch position of

the ball in order to determine the launch speed. The launcher would need to be able to launch a full scale model at a maximum speed of 80 mph with no rotation. To achieve the successful launch of the ball there were two options that we explored. Firstly, a pneumatic cannon which would pressurize air in a chamber, held back by an airtight valve. The ball itself would sit in the base of a large barrel, the air would be released from the pressurized chamber and would send the ball flying out of the barrel of the air cannon. This would allow us to achieve high exit velocities but would not allow us to have control of the ball's spin or orientation leaving the barrel.

The second option would be similar to a Jugs machine, commonly used in American football to launch the ball with a spiral. This machine operates by using two spinning rubber wheels on either side the gap between the wheels is slightly smaller than the ball. When the ball is pushed into the wheels, the friction will pull the ball through the wheels and out at variable speeds depending on the rotational speeds of the wheels. In order for us to recreate this mechanism we would need to buy two motors which spin at a high enough RPM to achieve speeds around 80 mph. The difficulty with this would be achieving the exact same speed and angle of the wheels in order to make the model have zero rotation through the flight.

While both of these options could be manufactured by the team, we figured that it would be exceedingly difficult to replicate the same launching orientation through all models. Wind or Water tunnel testing would be the most efficient method of testing simply because the ball's orientation would be much more manageable. Also the acquisition of two high speed cameras that would be able to track the small details of the flight was brought to question. Therefore, our team decided against the ball launcher project and moved forward with other experiment options.

Water Testing

The third and final choice for physical testing was performing a water test. Changing the fluid to water from air allowed us to achieve the same Reynold's number at a much slower speed. Since we did not have access to a water tunnel, we were left to find a body of water that we would be able to use for engineering purposes. The first place we investigated was the WPI rowing tank because this would simulate flow around the ball as it creates a natural stream of water. The rowing tank, upon inspection, only had approximately 6 inches of water which flowed erratically through the channel in which the water was contained. This small amount of water would make it so we would have to scale our models down so far that the flow velocity would be impossible to reach. Additionally, the ball would be too close to the floor of the tank and the surface of the water, making the flow non-uniform.

The WPI swimming pool was then the only body of water large enough to conduct an experiment of this scale. Unfortunately, the pool does not have a natural flow through it and that is why we needed to create flow around a ball. This can be created by either pushing water around the ball or pulling the ball through it. Due to our inability to create a flow of water in the pool, we created a system in which we would be able to pull the models through the stationary water at high enough speeds where we can notice changes in the ball's path to determine the change of flow and at which velocity that occurs.

To visualize the lift forces on the ball, we pulled physical models through the water in the WPI swimming pool in place of a wind tunnel. A 110V electric motor with a spool was used to pull the 3D printed model through the water. It had a maximum force of about 30lbs ($F_d = 1/2 \times \rho \times u^2 \times A \times C_d$). The electric motor had a horsepower of 2 and an RPM of 1800, giving us a torque of 5.8 ft*lb . The two testing spools had a cylindrical shape with a diameters of 1.867" and 1.494". The retrieval line was wound on the spools rotating at the same speed (1800 rpm)

but with different circumferences, in this way the ball could travel at a fast and a slow speed. The circumferences dictate that the ball would be pulled at a fast speed of 10 mph and a slow speed of 8 mph with a maximum force of 30lb. The 3D printed models were a 5:9 scale of a full size soccer ball, with this in mind our testing velocity was approximately double to account for the reduced diameter of the ball. The speeds of 8 and 10 mph in water represented air speeds for a full sized ball of 65 and 75 mph respectively.

The spools were created to fit the driveshaft of the motor with varying diameters to simulate different speeds. Using a series of calculations we picked two speeds that we wanted to pull the models at and then determined the circumference needed to reel in the line at those speeds. The table below displays the process used to determine spool size based on the desired speed in both water and air.

Speed in Air (mph)	Speed (mph)	Speed (m/s)	Rpm (in/hr)	Circumference (in)	Radius (in)	Diameter	Reynolds #	
91.27074067		12	5.364327224	760320	7.04	1.120451746	2.240903492	764713.7761
83.66484561		11	4.917299955	696960	6.453333333	1.027080767	2.054161534	700987.6281
76.05895056		10	4.470272687	633600	5.866666667	0.9337097881	1.867419576	637261.4801
68.4530555		9	4.023245418	570240	5.28	0.8403388093	1.680677619	573535.3321
60.84716044		8	3.576218149	506880	4.693333333	0.7469678305	1.493935661	509809.1841
39.98381001	5.2568	2.35	333070.848	3.083989333	0.4908325614	0.9816651229	335005.1738	

Figure 16: Spool Calculations

Although testing the models in water was to look into the aerodynamics of the ball, Reynold's number remained the same despite the fluid moving around the ball. This way we were able to calculate the required velocity needed to turn the flow of water around the ball turbulent. We were then able to set the acquired Re_{Water} value to the Reynolds number equation, subbing in the values for air and solving for the velocity needed to change the flow turbulence in the air. From the papers we had researched, our team expected the velocity in air to be approximately 80mph. Therefore:

$$Re_{air} = \frac{(80mph)(9")}{1.516*10^{-5}} = Re_{water}$$

Solving this equation for the velocity required from the Re_{water} equation we attain an expected velocity of 10.8 mph. Our test needed to accommodate this and pull our models with a range

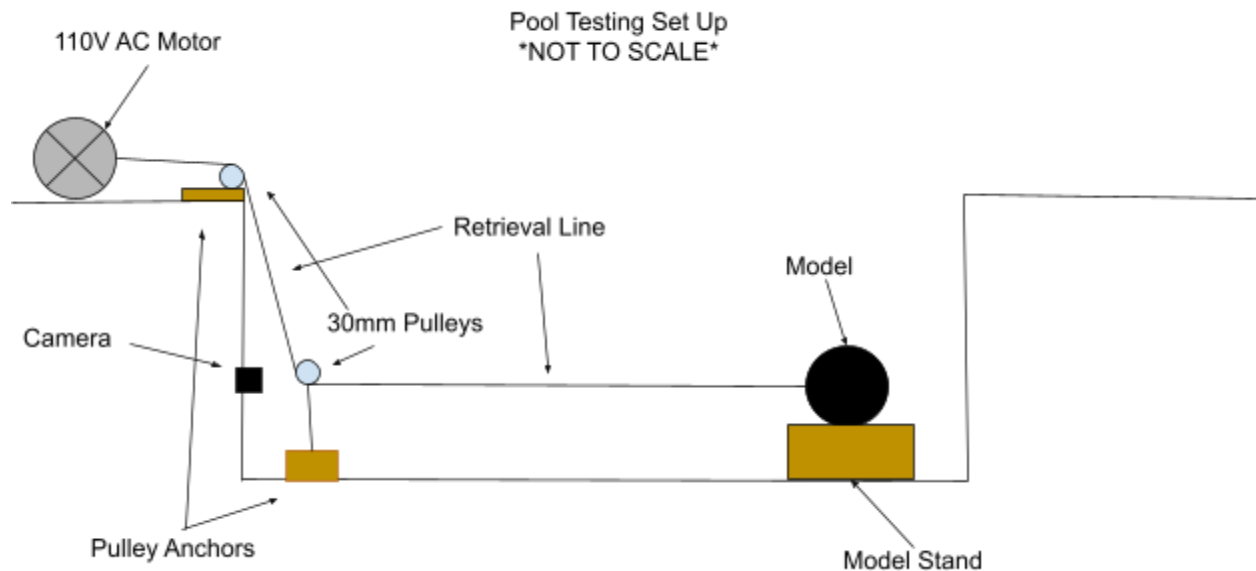


Figure 17: Diagram of the Pull Test

The retrieval line pulled the ball with a series of pulleys, one located before the line enters the water at the edge of the pool, and another mounted approximately two feet above a rubber weight placed on the floor of the pool. This gave the ball sufficient distance from the floor of the pool as to not affect the flow behavior. In order to observe the ball's motion, a camera was mounted just below the submerged pulley, allowing the ball's vertical and horizontal movement to be captured and analyzed. The ball was placed opposite and level with the camera, allowing the camera to pick up the ball's entire flight path and to prevent the pull point from influencing the initial velocity of the ball in any direction besides the X-axis.

The balls were designed to be as closer to neutrally buoyant as possible, while still remaining partially negative. This ensured the ball did not drag across the floor of the pool or float to the surface. The 3D printed model had a volume of 65 cubic inches and displaced

approximately 2.319lbs of water. The balls were printed with a 15% infill with a final weight of approximately 0.5lbs. From there two pound weights were added to the model, and the models were around 2.5lbs. The two pound weights are selected due to time constraints as that is what was readily available, easy to put in, and met our constraints. While the partially negative ball would sink while stationary, the calculated Froude number is supercritical, meaning the forces of the water on the ball greatly exceed the gravitational forces on the ball ($Fr = v / (g hm)^{1/2}$). This means that the ball traveled as if neutrally buoyant even if it is slightly negative.

It was planned that each model be pulled three times at each speed. Three tests would make our results more robust. It would reduce the impact of variability on the test results and make them more viable. More than three tests would produce more accurate results, but the time it would take to do this exceeded what was available.

Design Constraints

When evaluating the behavior of a soccer ball, a number of design elements come into play. From those existing elements, we chose the variables that we deemed the most important to test: seam length and depth, ball surface, and panel symmetry. Additionally, we broke ball behaviors down to the two most important non-dimensional variables: the critical Reynolds number and the drag coefficients. While most papers focus on ball behavior as it relates to spin or ball orientation, there is some existing data that compares various ball constructions. Note that the effects of spin were often not isolated from the potential impacts of design changes.

Simulation Data

Smooth Ball

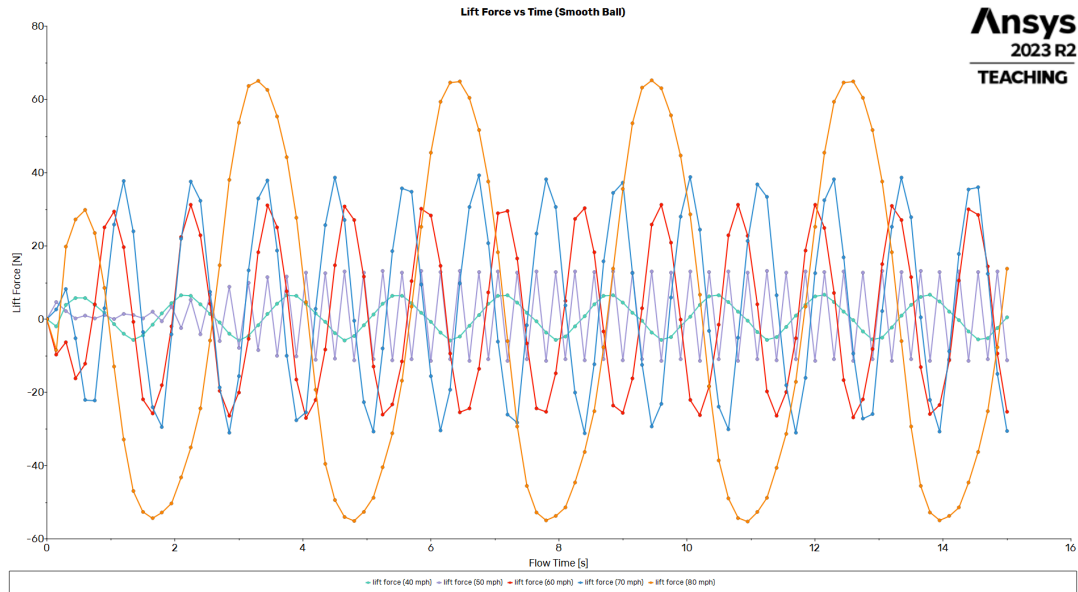


Figure 18: The lift force vs flow time of the smooth ball model. All speeds are presented on one graph to convey the effect the change in speed has on the lift forces of the ball.

The smooth ball data was the first data acquired for the project. Since the aerodynamic behavior of a smooth ball is well understood, it was easy to tell when a simulation was set up incorrectly: if there were no waves for the smooth ball, the simulation was not set up in the correct way. As shown in Figure 18, wave behavior was observed for all speeds. Additionally, the wave was expected to increase in amplitude as the wind speed increased, which was shown to be the case.

Dimpled Ball

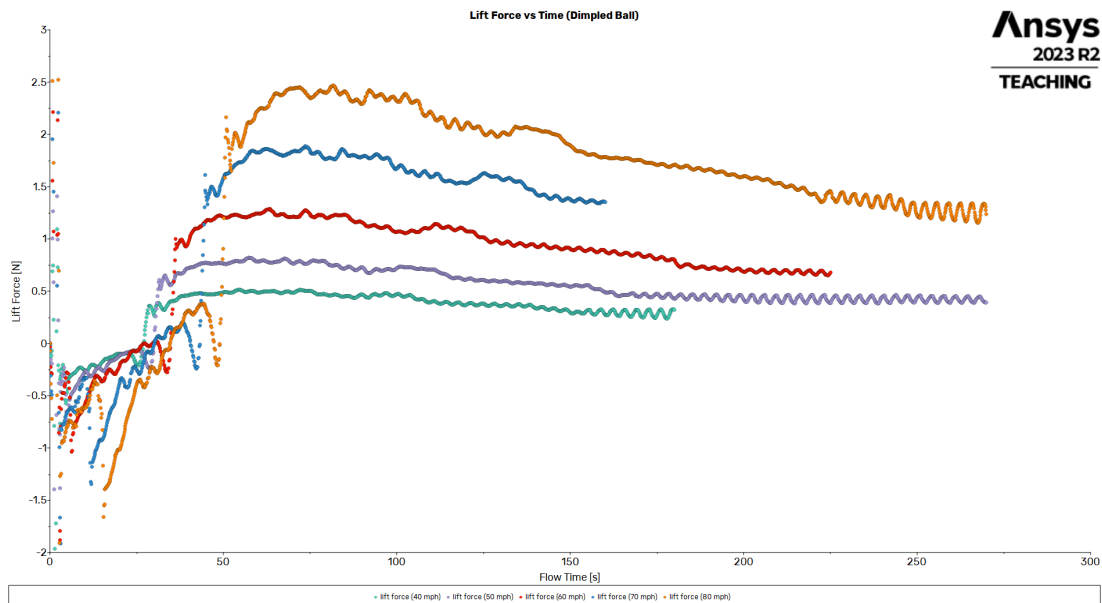


Figure 19: The lift force vs flow time of the dimpled ball model at all speeds. Each simulation was only run for the amount of time needed to reach convergence, which is why the lines are different lengths.

The dimpled ball served as both a test of ball surface texture and a second control. Golf ball aerodynamics have been studied more than soccer ball aerodynamics, so there was once again an expected behavior in the force diagrams. If regular sinusoidal behavior was not observed late in the flow time, then the simulation was not set up correctly. The lift force also needed to be significantly lower for the dimpled ball when compared to the smooth ball at all speeds, which was found to be the case. Figure 19 highlights this.

32 Paneled Balls

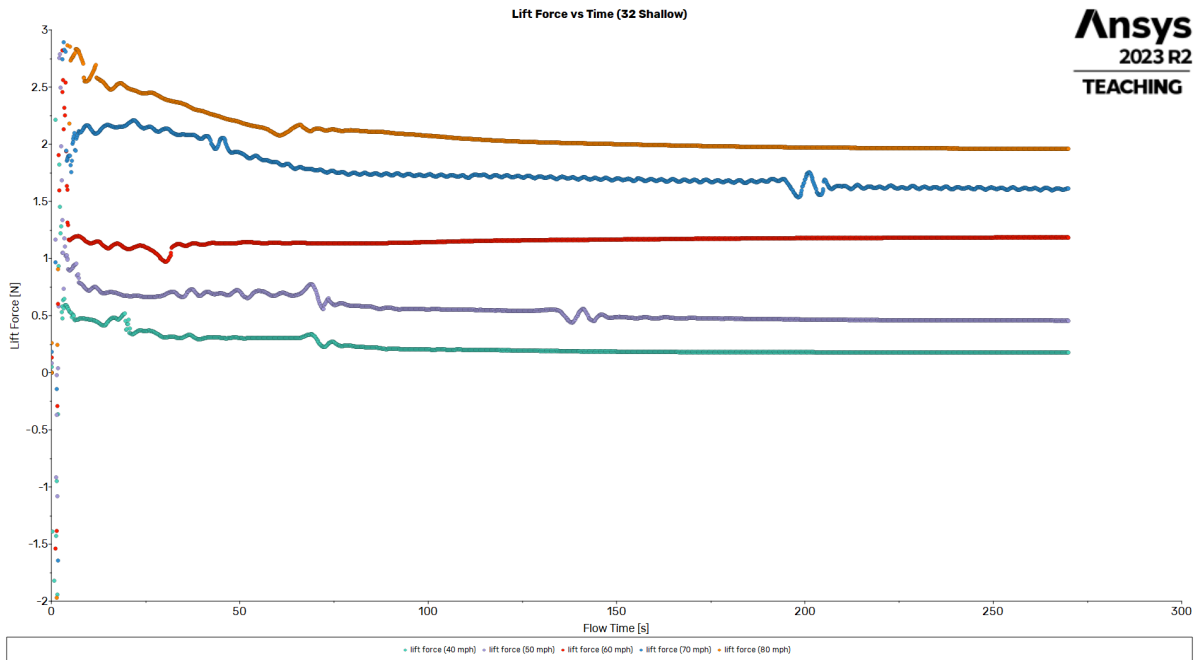


Figure 20: The lift force vs flow time of the 32 paneled ball with shallow seams model at all speeds. The y-axis scale was chosen for ease of comparison between all models, and thus not all wave patterns are visible.

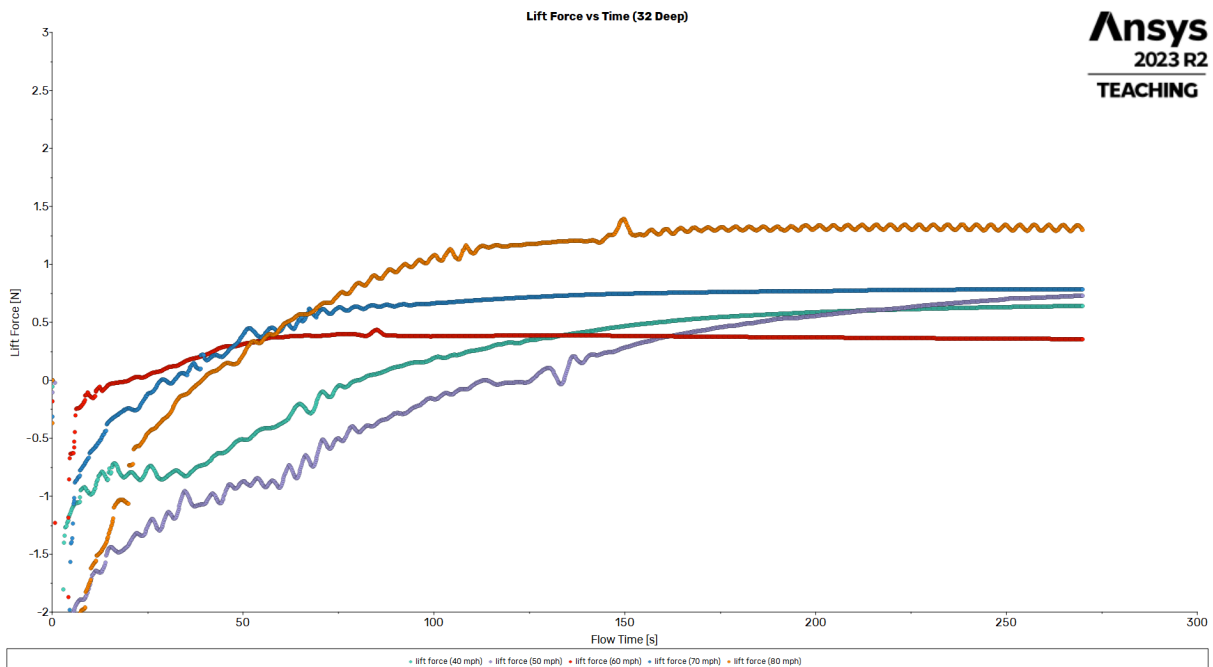


Figure 21: The lift force vs flow time of the 32 paneled ball with deep seams model at all speeds. This graph is scaled to the chosen y-axis, cutting off the information at the start of the flow behavior.

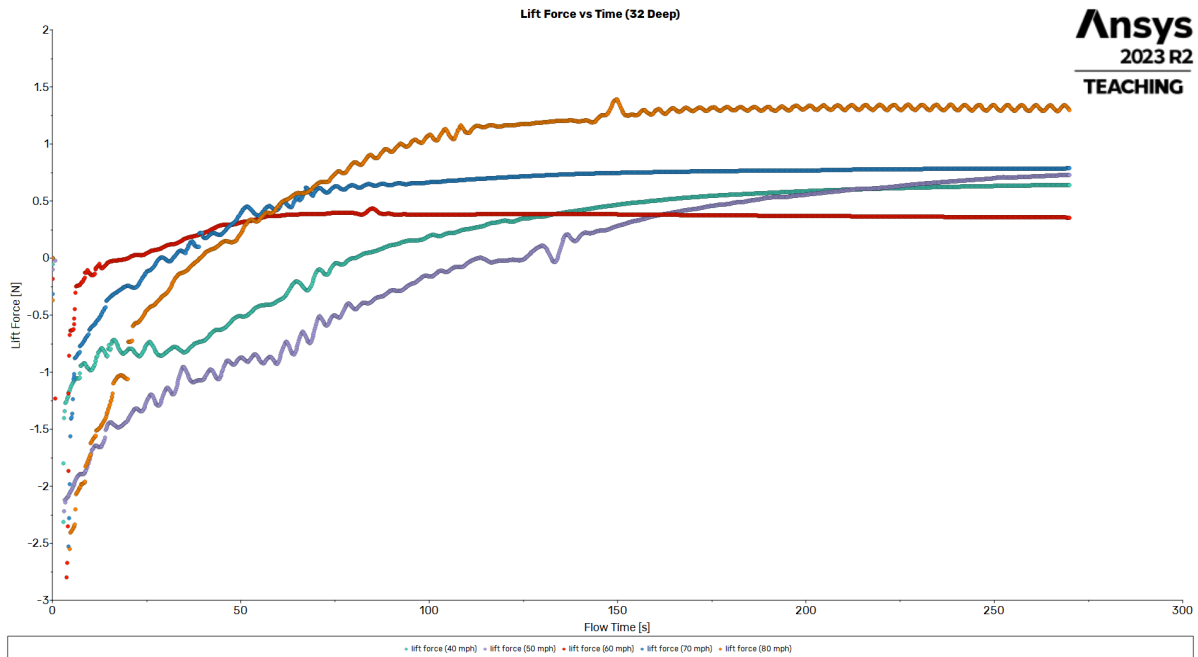


Figure 22: Lift force vs flow time of the 32 paneled ball with deep seams model at all speeds, with the y-axis scaled to show force data at the beginning of the flow time.

The 32 paneled balls did not behave as expected at all speeds. While the force averaged closer to 0 Newtons along the entire flow time, as well as peaking below the largest lift force present in the shallow seam model, there was a larger absolute difference between the smallest force value and the largest for the deep panels. However, at higher speeds (50 through 80 mph), the model with deep seams performed better than the shallow seamed model. The difference in the largest forces can be seen between Figures 20 and 21, but the larger absolute difference led to a revised y-axis scale for Figure 22. Further analysis of the testing time frame, which displayed similar results, is located in the following sections.

64 Paneled Balls

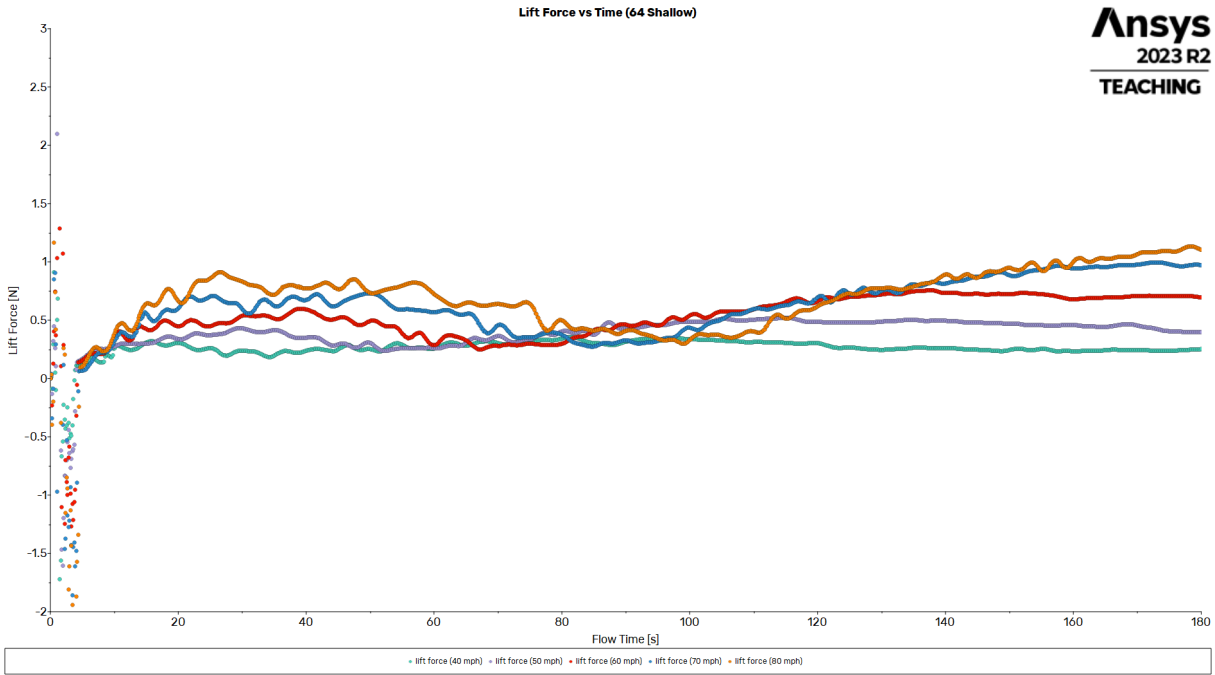


Figure 23: The lift force vs flow time of the 64 paneled ball with shallow seams model at all speeds.

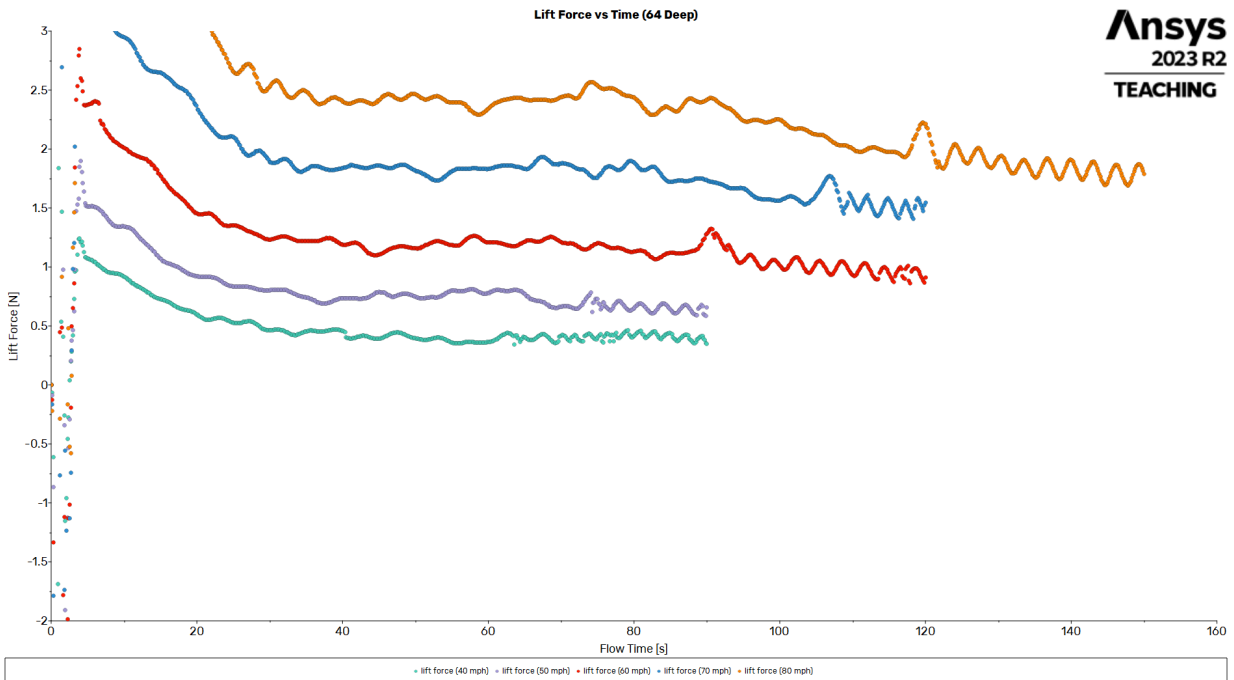


Figure 24: The lift force vs flow time of the 64 paneled ball with deep seams model at all speeds. This graph is shown with the y-axis scaled for comparison.

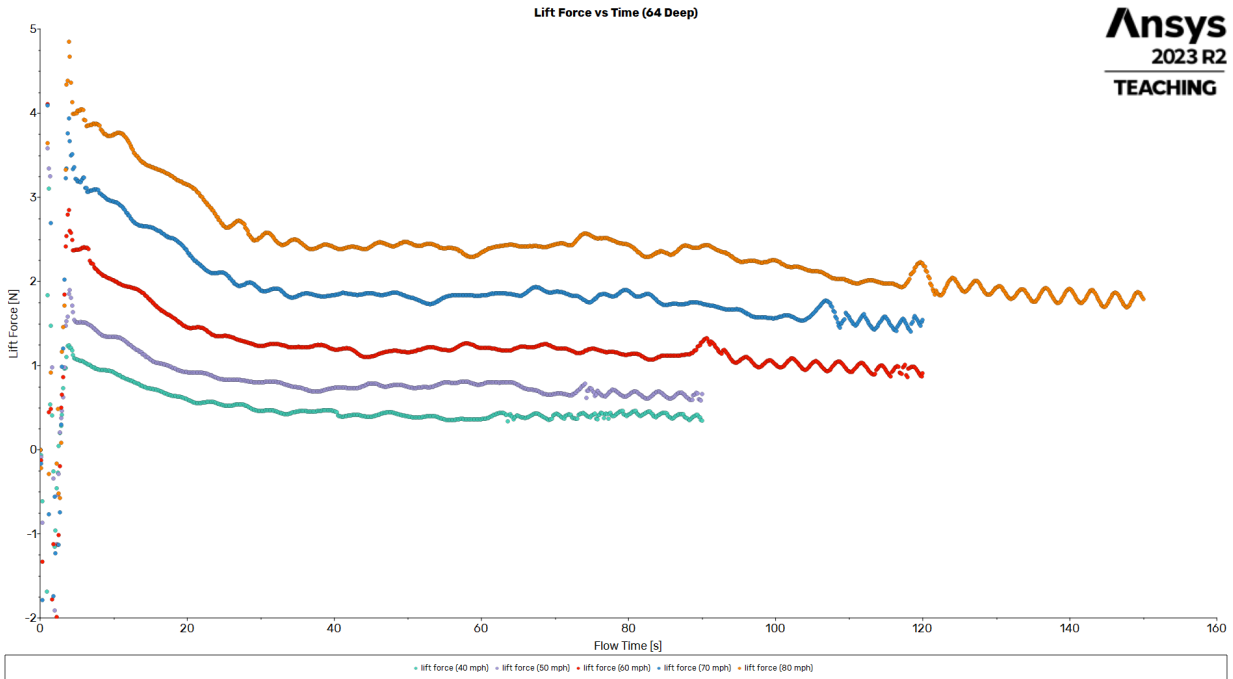


Figure 25: The lift force vs flow time of the 64 paneled ball with deep seams model at all speeds. This graph is shown with the y-axis scaled to visualize forces at earlier flow times.

The long term flow behavior of the 64 panel balls was consistent with expectations. In Figures 23 and 24, the overall force comparisons are clear. Once again, the model with deep seams was shown to have a higher overall force value, but a relatively smaller difference between the highest and lowest values. Figure 25 again contains a different y-axis scale to show the force present at earlier flow times. Over the longer flow time, the model with deep seams displayed behavior similar to the dimpled ball, which indicated a tendency towards long-term stability.

Model Comparisons - 60 mph

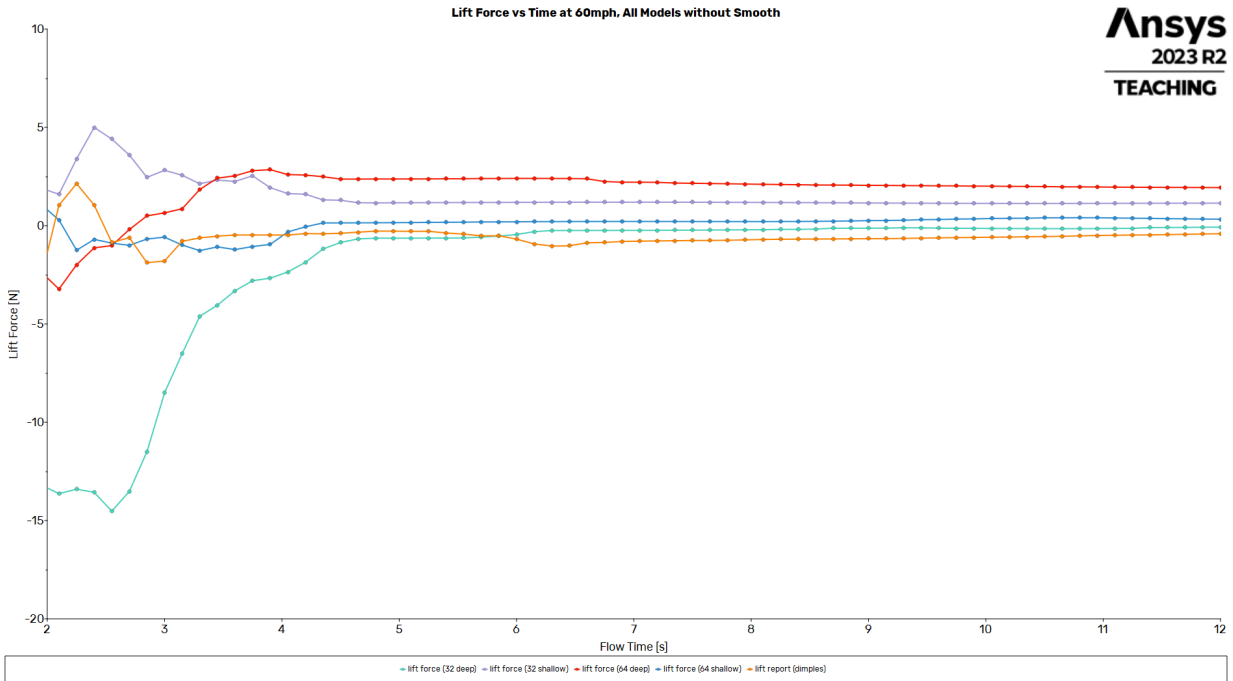


Figure 26: The lift force over a timeframe of 10 seconds of all models except the smooth ball at 60 mph. The timeframe used is 2-12 seconds of flow time, with the simulation setup portion taking place from 0-2 seconds. This corresponds to the 0-10 second timeframe used for the physical simulation analysis.

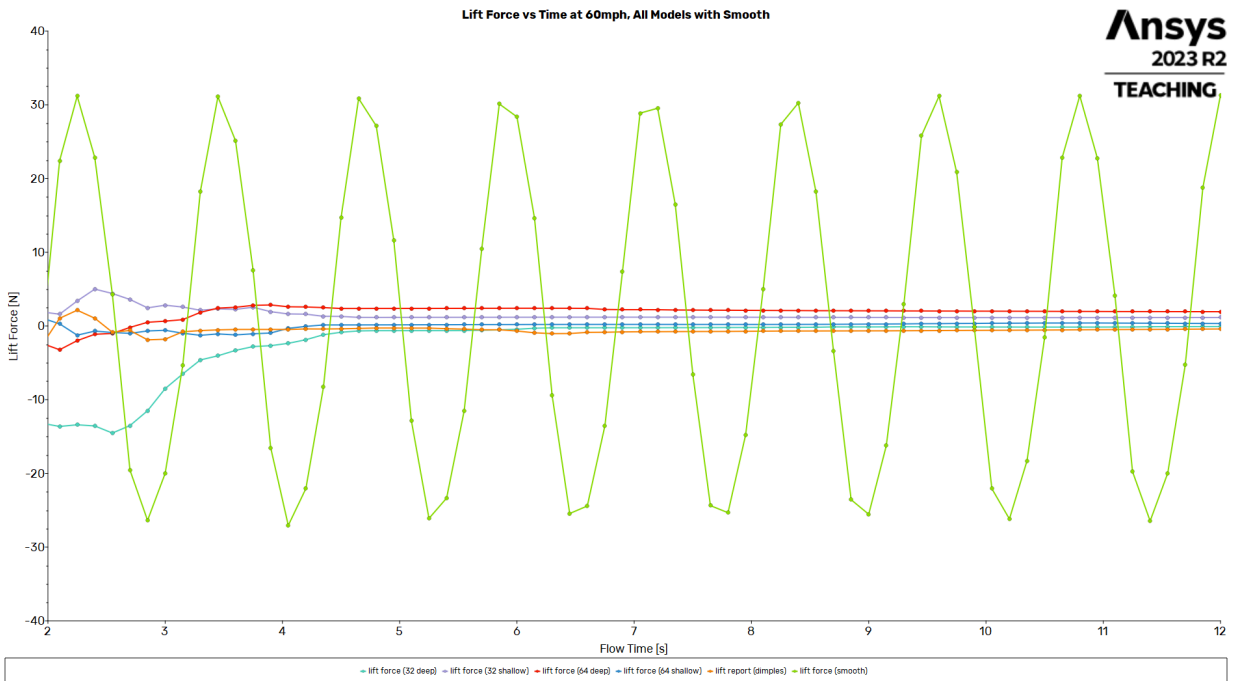


Figure 27: The lift force over a timeframe of 10 seconds of all models at 60 mph.

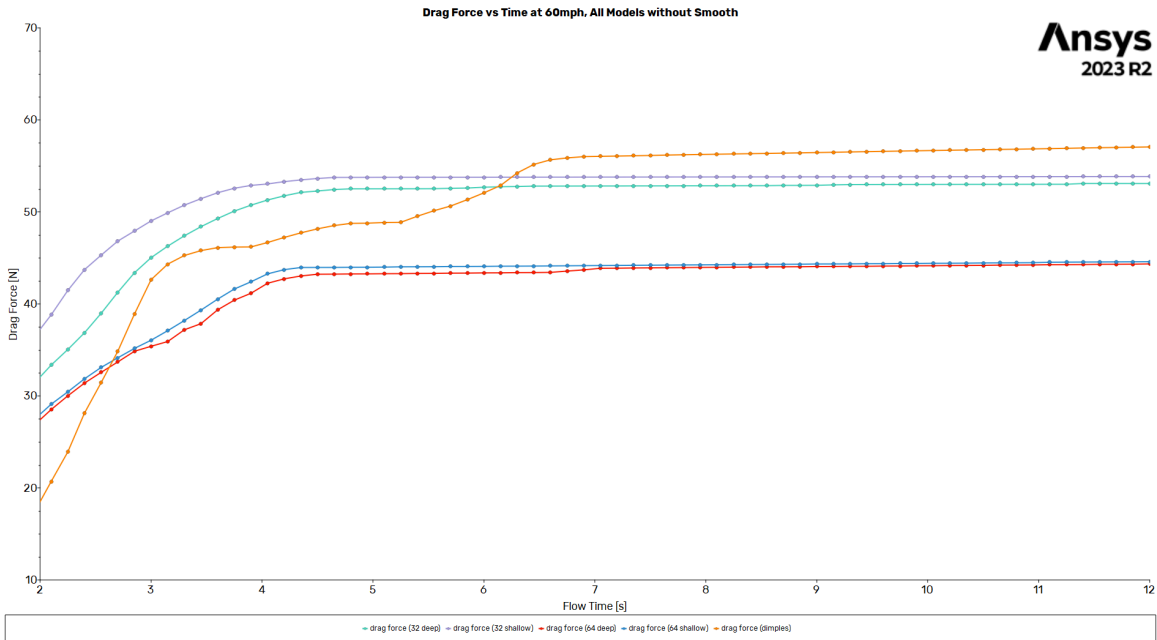


Figure 28: The drag force over a timeframe of 10 seconds of all models except the smooth ball at 60 mph.

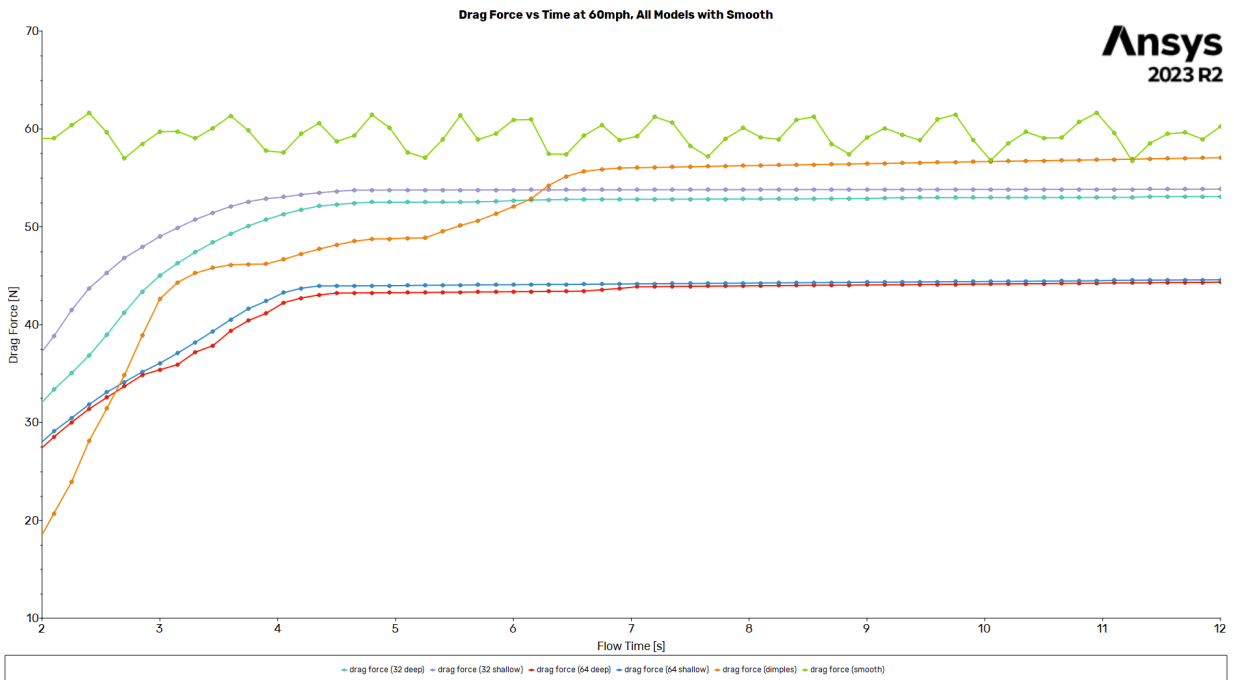


Figure 29: The drag force over a timeframe of 10 seconds of all models at 60 mph.

Model Comparisons - 80mph

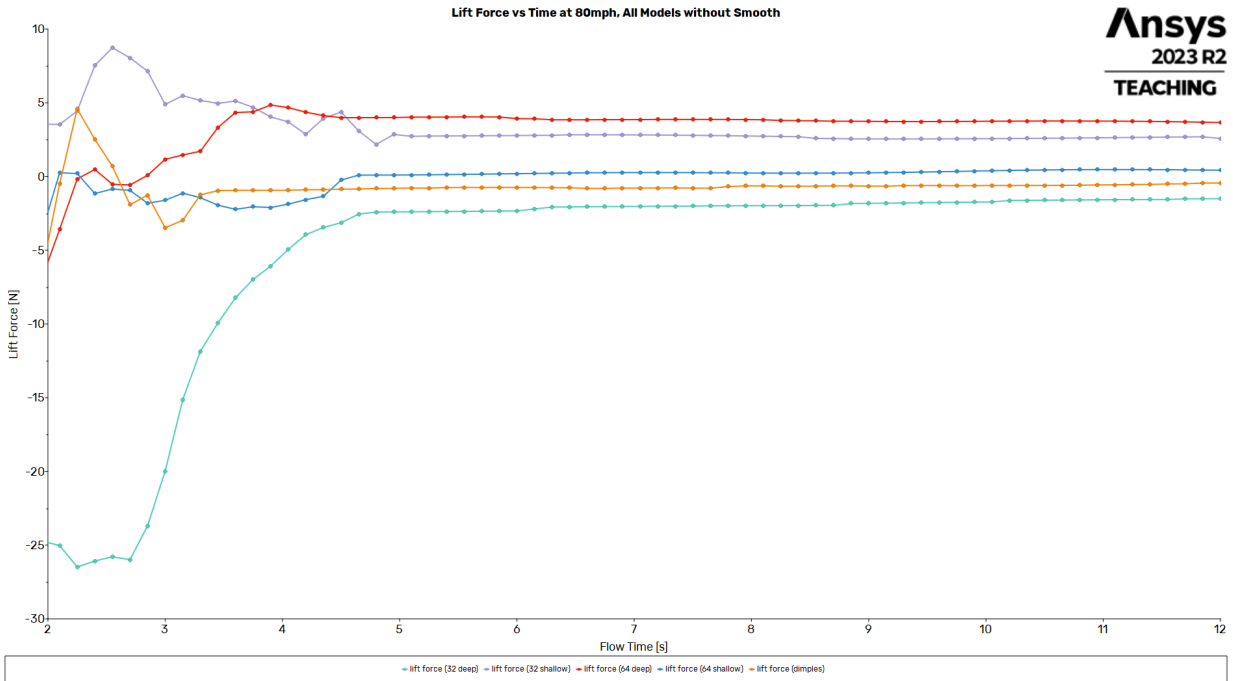


Figure 30: The lift force of all models except the smooth ball at 80 mph over a timeframe of 10 seconds.

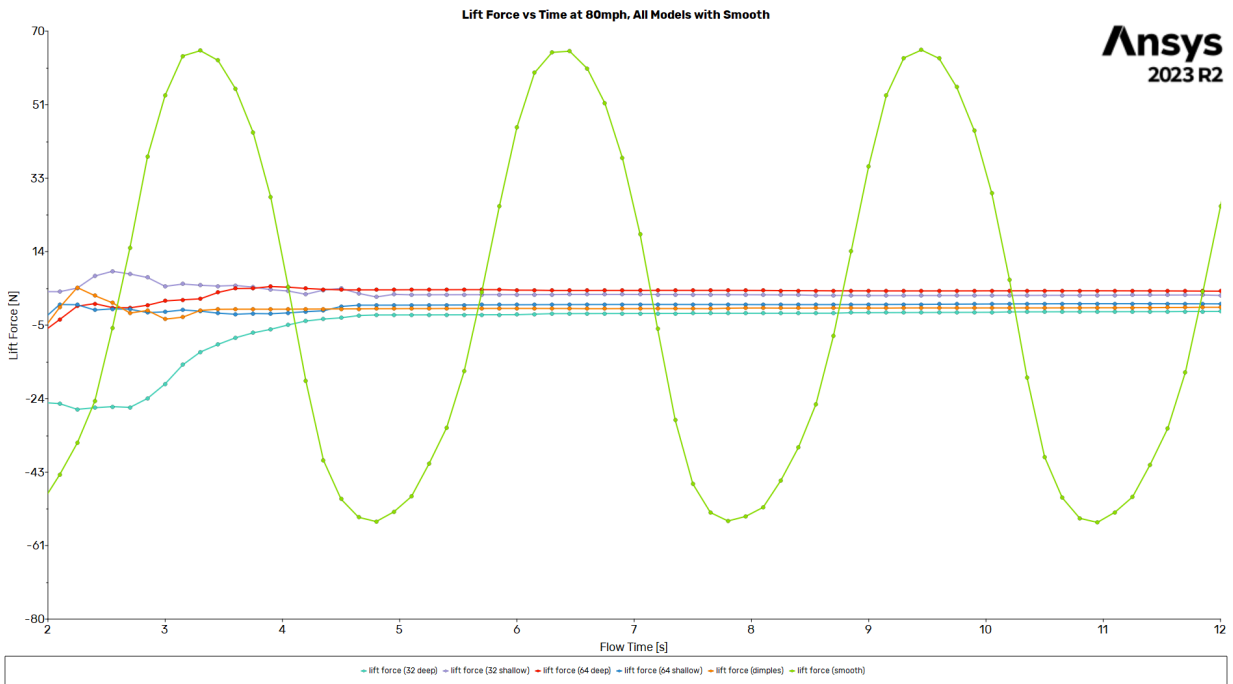


Figure 31: The lift force of all models at 80 mph over a timeframe of 10 seconds.

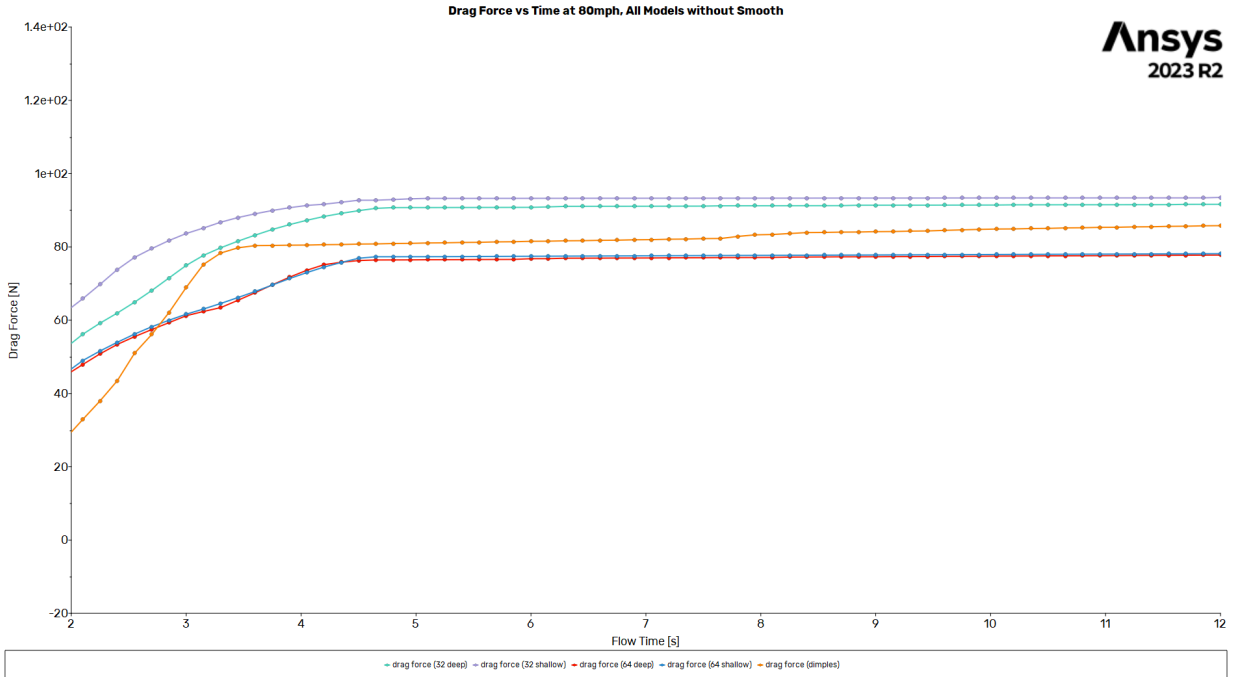


Figure 32: The drag force over a timeframe of 10 seconds of all models except the smooth ball at 80 mph.

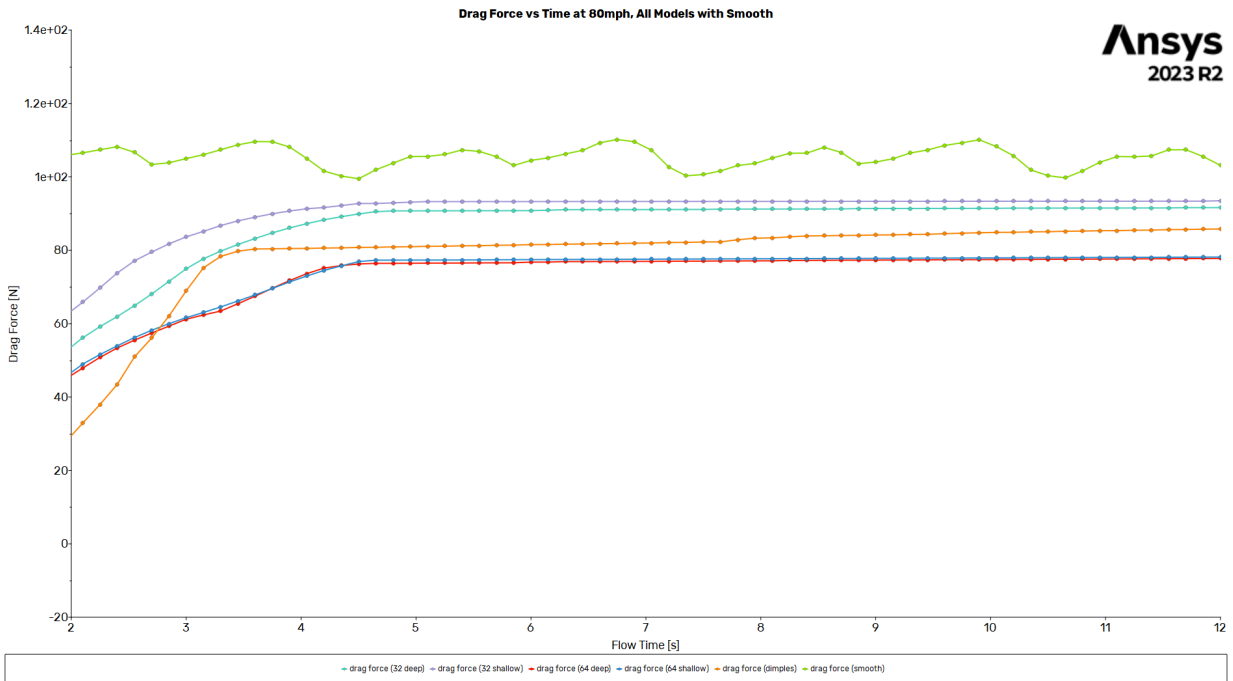


Figure 33: The drag force over a timeframe of 10 seconds of all models at 80 mph.

Water Testing Results

The following figures are used to represent the overall displacement of each ball model throughout the experiments. As previously stated, each model is pulled at 8 and 10 mph to represent 60 and 75 mph in air respectively. The balls are pulled from the origin of the graphs and visualize the balls' flow path through the water in each test. The ball that has the most displacement through a test indicates more lift forces on the ball, and therefore higher knuckling. Conversely, the balls that do not displace from the X-axis have minimized knuckling and lift forces. This way we are able to compare visual data to the received simulation data to determine which design characteristics of a soccer ball minimize the knuckling effect.

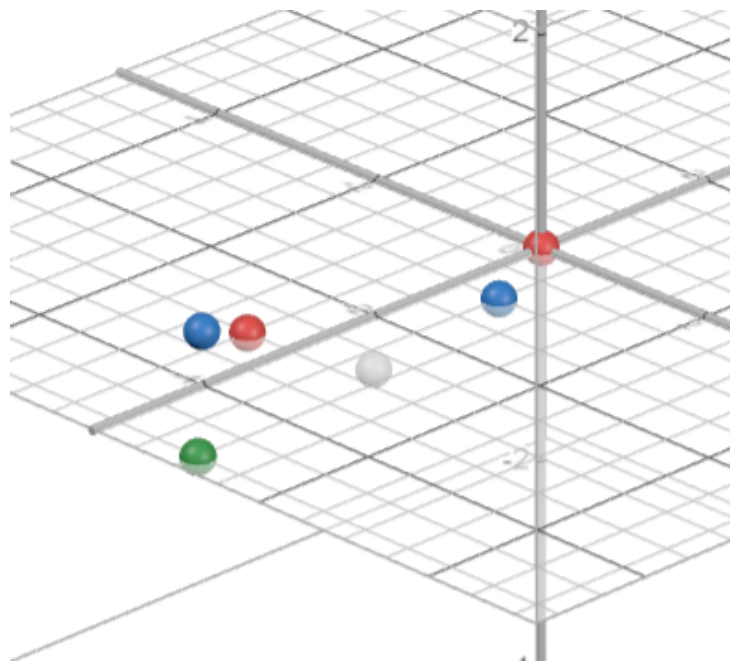


Figure 34: 32 Panel Deep Seam (8 mph)

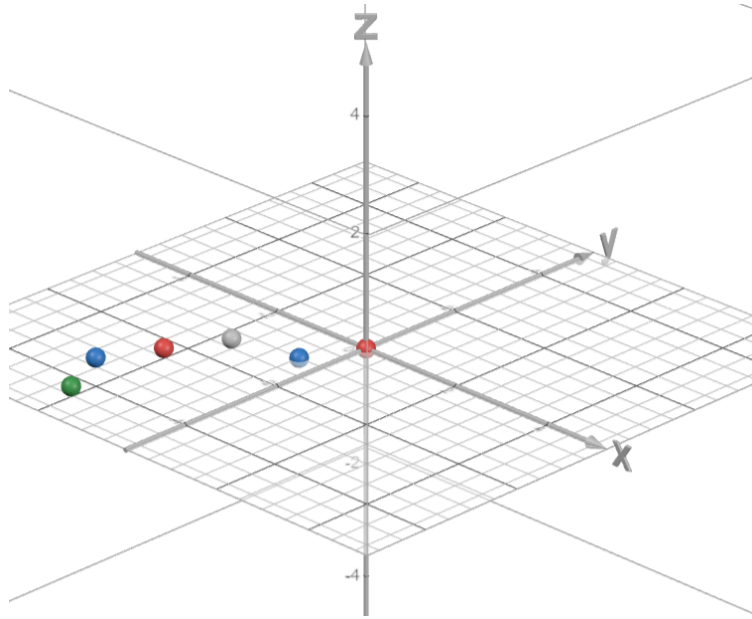


Figure 35: 32 Panel Deep Seam (10 mph)

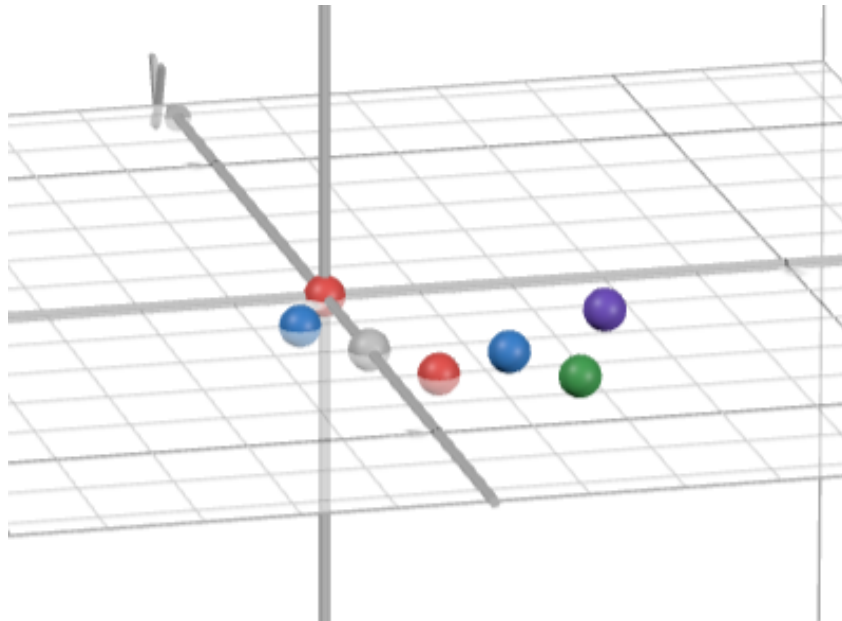


Figure 36: 32 Panel Shallow Seam (8 mph)

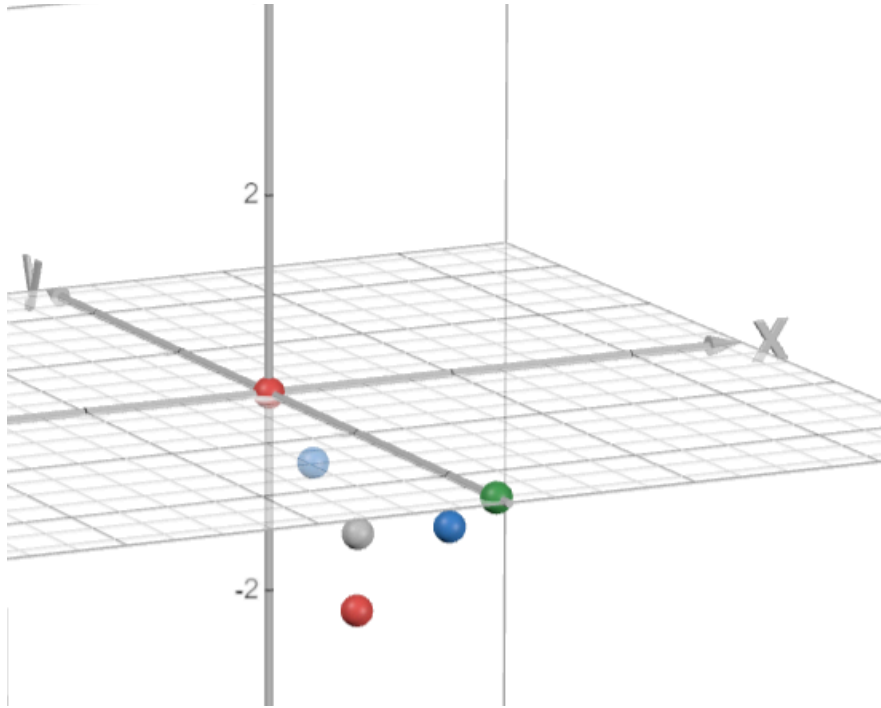


Figure 37: 32 Panel Shallow Seam (10 mph)

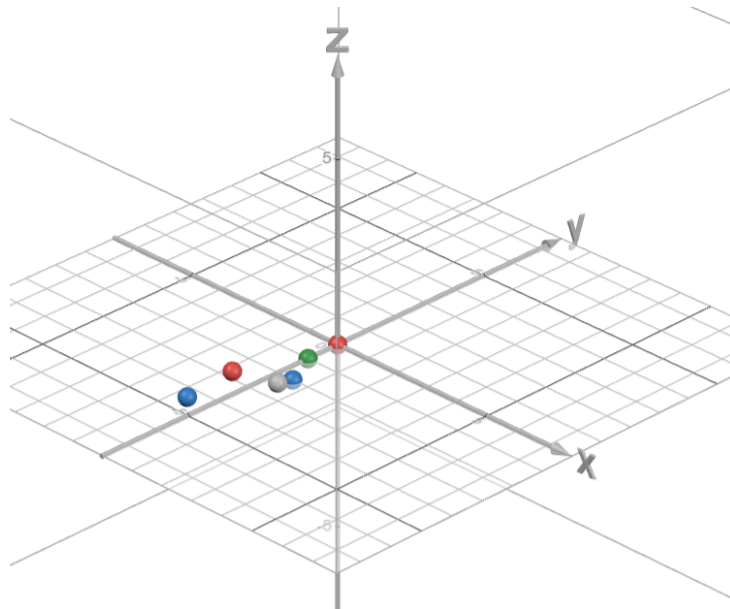


Figure 38: 72 Deep Seam (8 mph)

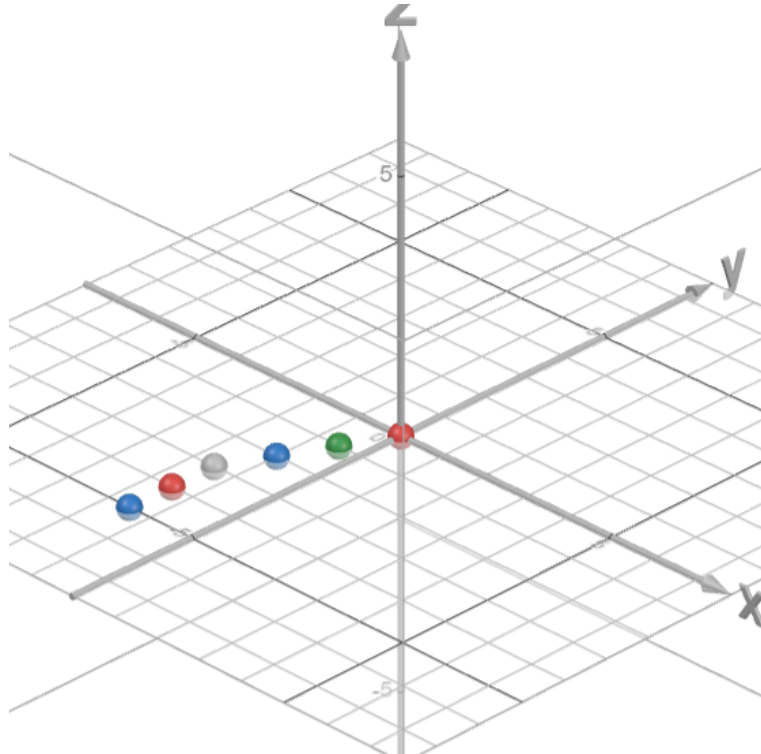


Figure 39: 72 Panel Deep Seam (10 mph)

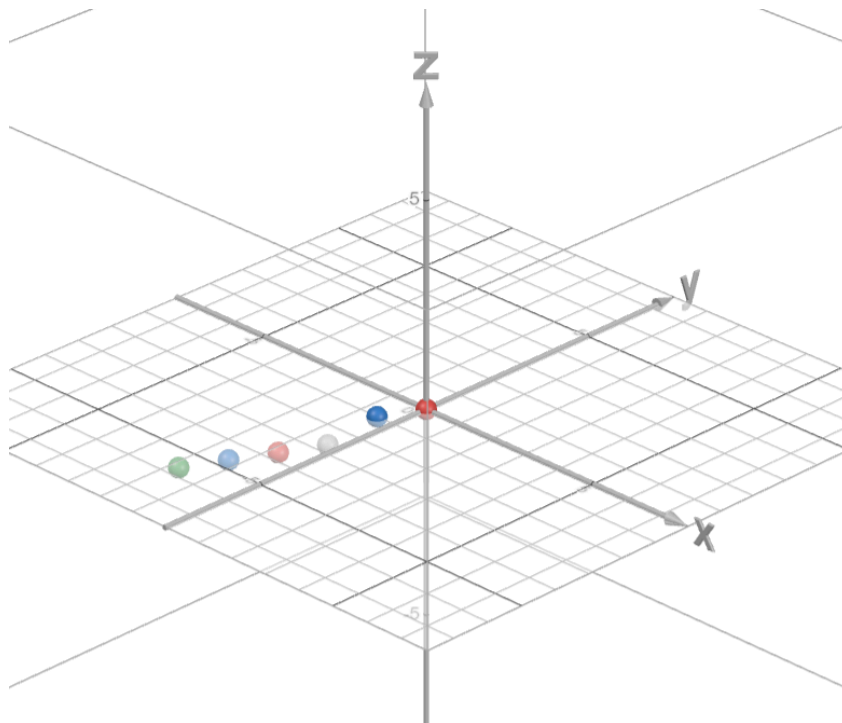


Figure 40: 72 Shallow Seam (8 mph)

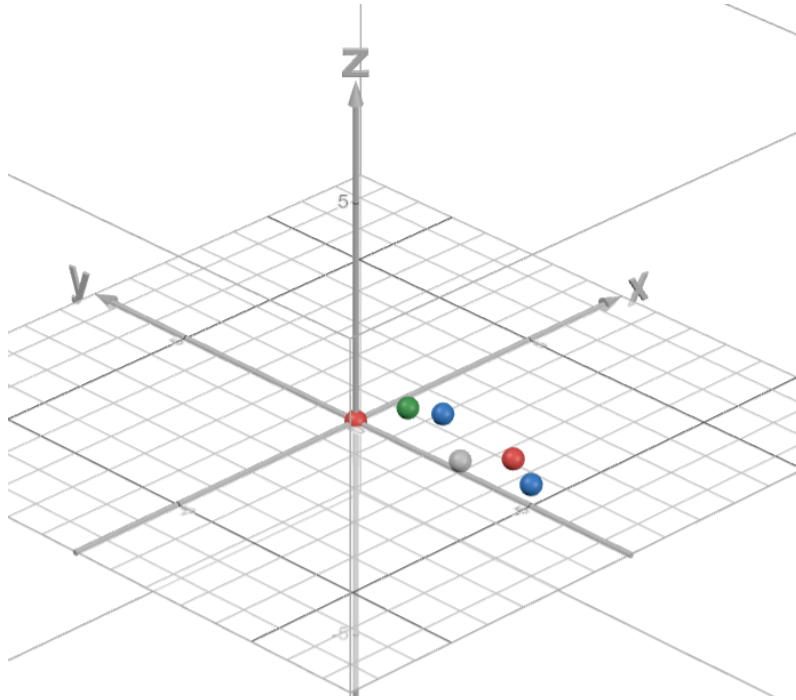


Figure 41: 72 Shallow Seam (10 mph)

Discussion

Wind Tunnel Simulations

Across all geometric variations, the smooth ball had significantly larger differences in both the lift and drag forces. To visualize the differences in lift force between each model, a bar chart was created for each speed test.

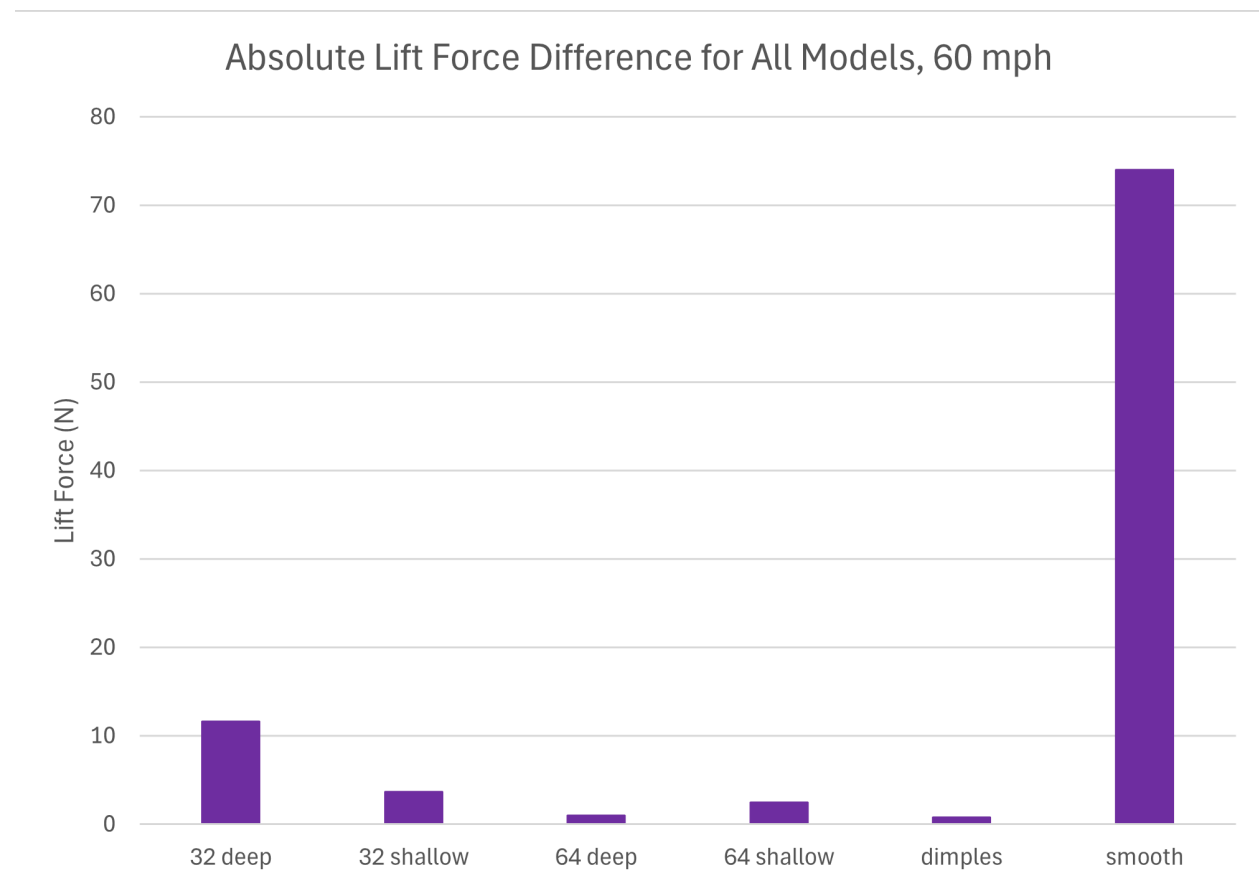


Figure 42: The physical representation of the lift force differences from time = 0s to time = 10s for all ball models at 60 mph. The data used to complete this graph was taken from the data points shown in Figure 26, and the table containing that data is located in Appendix B.

At 60 mph, the trends in the largest and smallest lift forces are highlighted in Figure 42. There was an unexpected decrease in lift force between the 32 deep and the 32 shallow models, going against the expected result. However, all other models behaved as expected: the smooth ball showed a significantly larger difference, the dimpled ball had the smallest difference over

the testing time frame, and increasing the number of seams reduced the force difference in both shallow and deep seam cases. For a visualization of the largest and smallest forces for each model, refer to Appendix B.

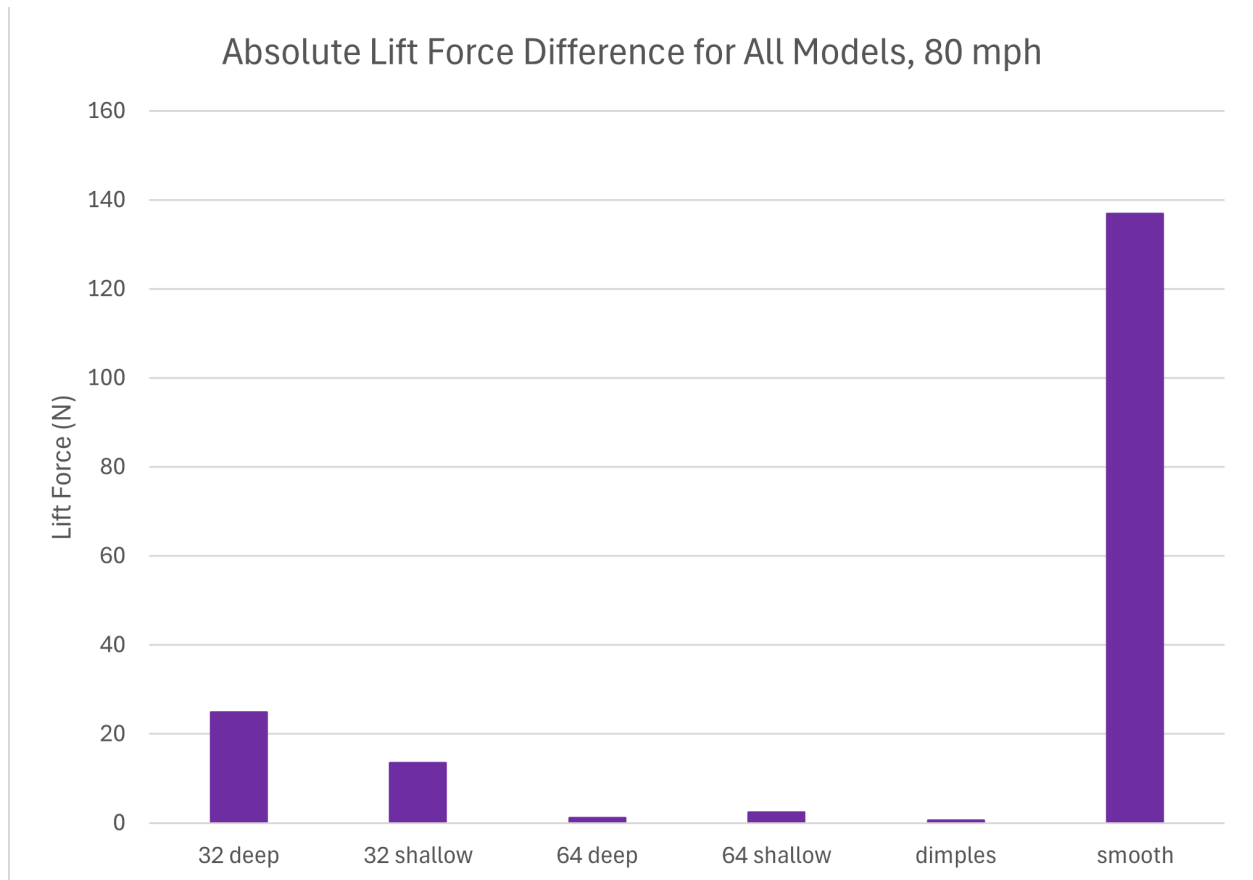


Figure 43: The physical representation of the lift force differences from time = 0s to time = 10s for all ball models at 80 mph. The data used to complete this graph was taken from the data points shown in Figure 31, and the table containing that data is located in Appendix B.

Figure 43 represents the same data, but for the tests that took place at 80 mph. All force differences increased due to the larger wind speed, but the behavior remained the same for each ball model. For a visualization of the largest and smallest forces for each model, as in the 60 mph case, refer to Appendix B.

In general, the addition of seam length resulted in a consistent decrease in force difference, which was in line with our general expectations. The impact of seams on

aerodynamic performance suggests a nuanced relationship between seam length and airflow dynamics. Furthermore, dimpled balls exhibited the smallest changes in lift forces over our selected timeframe, highlighting their potential as a design choice for maintaining consistent aerodynamic behavior across different speeds. While this behavior is not consistent over longer timeframes, that data is not relevant to our model analysis. Rather, it serves as a way to confirm simulation consistency and make more general assumptions about airflow.

Interestingly enough, the transition from shallow to deep seams in 32 panel ball models led to an unforeseen increase in force. This counterintuitive observation raises questions about the airflow interactions with seam depth, as well as contrasting with the physical testing data. There are a number of potential reasons for this. The model could have been built in such a way that the 2D slice did not result in a symmetrical design. This asymmetry is known to increase lift forces (19, 20). The 32 panel, deep seam mesh was also one of the first meshes created, so there is a possibility of a meshing error that went undetected. However, the model performed as expected when looking at drag forces, which suggests that the issue is not with the model itself. Looking beyond, this result suggests that deeper seams may introduce complexities in airflow patterns, potentially disrupting the expected reduction in aerodynamic lift forces.

As far as the goals of simulation testing (quantitative analysis and predictions for physical testing behavior), both were met. Since a consistent and accurate methodology was established, quantitative data could be successfully evaluated even though the simulations were not true to life. Additionally, we were able to use that quantitative data to form relatively accurate hypotheses on the outcomes of our physical testing.

Water Testing

As the models were subjected to increasing speeds during testing, there were noticeable differences in their flight path, in terms of knuckling. At higher velocities, the models exhibited higher knuckling, indicated by greater erratic movement patterns. This was determined based on the visualizations of the ball movement through the pull. For each model, the displacement was higher when the ball was being pulled at 10 mph rather than 8. This confirmed that increased speed increased lift forces on the ball.

The knuckling effect was especially pronounced with the smooth ball model, where the absence of surface texture caused the erratic flight path. The model experienced the highest lift forces during testing and the forces applied to the smooth ball model were so intense that they caused the ball to fracture, which was not observed in any other tested model. Before the ball fractured and the test was voided, the ball moved 5 feet in the positive X direction, which was a wider variance than any other model tested. These results were seen during the 8 mph test, meaning that if the ball was able to be tested at 10 mph the knuckling would have been even more severe than what was depicted.

The golf ball model stood out with the most promising results, supporting the importance of surface texture in aerodynamic performance. This ball barely moved off the X axis during both pulls, promoting the idea that the more surface texture on a model means that the knuckling effect was minimized. This hypothesis was conceived because a golf ball has several deep seams all across the ball.

To continue to prove this theory, the models with deeper seams and longer seam lengths notably decreased lift forces, contributing to enhanced stability and control during flight. These design characteristics showed to be effective in minimizing erratic movement, enhancing the

models' performance at various speeds. This is seen through the figures above that depict the flight path of each model. The overall displacement of the 72 panel with deep seams was a total of 1.5 feet of movement. This was the least that was seen in all models, confirming the idea that the increased amount of surface texture means minimized knuckling effect. Conversely, the 32 panel with shallow seams displaced 7 total feet, the most of any other model. When comparing just seam depth, the 32 panel deep seam at 10 mph (Figure 39) moved much less than 32 panel shallow seam at 10 mph (figure 38), this is true for both speeds. This is also the case for the 72 panel ball seen in figures 41 and 43.

From our results, it can be theorized that deeper seams, longer seams, and surface texturing increase the predictability of the flight path of the ball. The inverse of this can also be theorized: that the more perfect the sphere, the more unpredictable the flight path becomes. Moving forward with the results would point to testing models with even more surface features in order to determine the extent of the effectiveness of surface features on the predictability of a ball's flight path.

Broader Impacts

Engineering Ethics

While our goals may stand in opposition to financial goals of existing ball manufacturers by advocating for a standardized ball design, we believe it aligns with broader ideals of excellence in soccer. These ideals include upholding the integrity of the game, promoting fair competition, and ensuring that competition winners are determined by skill and strategy rather than chance. With over 5 billion spectators tuning in for the 2022 World Cup, our efforts will not only help professional soccer leagues, but also across global audiences, ultimately shaping perceptions and expectations around professional soccer.

Societal and Environmental Impacts

Our decisions carry societal and environmental implications as well. By adopting a universal soccer ball design, production processes can be more effectively streamlined. A universal ball design would also help reduce environmental waste in the long term. Although the immediate environmental footprint of the product remains comparable to existing soccer balls, the transition to a single standardized design across all levels and leagues presents an opportunity to significantly reduce the ecological burden associated with manufacturing and distribution. Additionally, standardizing the design could result in fewer balls in circulation, as teams may choose to practice with balls that use the competition design only. This would result in less waste being generated.

Codes and Standards

Due to the uniqueness of our project and form of physical testing certain safety standards were adopted in order to prevent harm to any individuals involved in experimentation. Standards and guidelines were taken from ASSP and ANSI. Before we began any testing in the pool area, a safety and risk analysis was conducted. This analysis highlighted three main issues that needed to be addressed, electricity, swimming, and equipment. The setup that we used includes a 110V motor attached to a wooden board on the pool deck, when dealing with electricity in close quarters to water we needed to take precautions. The motor both had an internal thermal breaker as well as being plugged into a ground-fault circuit interrupter outlet, which would immediately cut power to the motor. The second thing we needed to ensure was the safety of the swimmer in the pool. For this the swimmer underwent a swim test by the lifeguards to confirm their ability to swim, additionally we had lifeguards attending each experiment to watch over the swimmer in case of unforeseen circumstances. Lastly, this test required a person to guide the fishing line on the spool so the line stayed on the spool through the pull. Holding onto the fishing line being pulled in at 10 mph causes a lot of friction, to prevent friction burn we wore industrial grade safety gloves.

Economic Factors

Economic factors include both the development and sales of balls, as well as revenue associated with major events such as the World Cup. As mentioned previously, by creating a universally used ball, that would reduce the number of types of balls being produced and sold. It could allow one ball manufacturer to dominate the market, raising another question around the ethics of mass production. The 2022 World Cup generated over \$7.5 Billion, with the host

country receiving about \$1.6 Billion (32). This does not account for the revenue generated by local shops and vendors that benefit from the influx of people.

Conclusions

In this study, we conducted wind tunnel simulation tests and water tunnel tests on various ball models to investigate the impact of the ball's surface on its aerodynamics. We compared the aerodynamics of the simulation and water tunnel models to determine which ball characteristic mitigates lift forces the most within the given kicking speeds in soccer. The tests show that the textured ball models have a higher level of dependence on the seam length and depth, and that these differences can produce significant changes in the drag and lift forces. The ball characteristics that mitigated the lift forces the best were shown to be the models with deep seams and longer seam length. These factors cause the ball to have more symmetry, no matter the panel orientation, which mitigates the fluctuating lift forces at various speeds. Testing also showed that the rougher models allow the surrounding air to transition from laminar to turbulent flow. Inducing an early drag crisis means that the balls have less drag when they are kicked especially at higher speeds, also helping to reduce asymmetric lift. Since the smooth ball transitions in flow later, the lift forces are most prevalent at these high kicking speeds and are indicative of knuckling. The dimpled ball exhibits all the desired traits and is shown within the test to have a more uniform and stable flight.

References

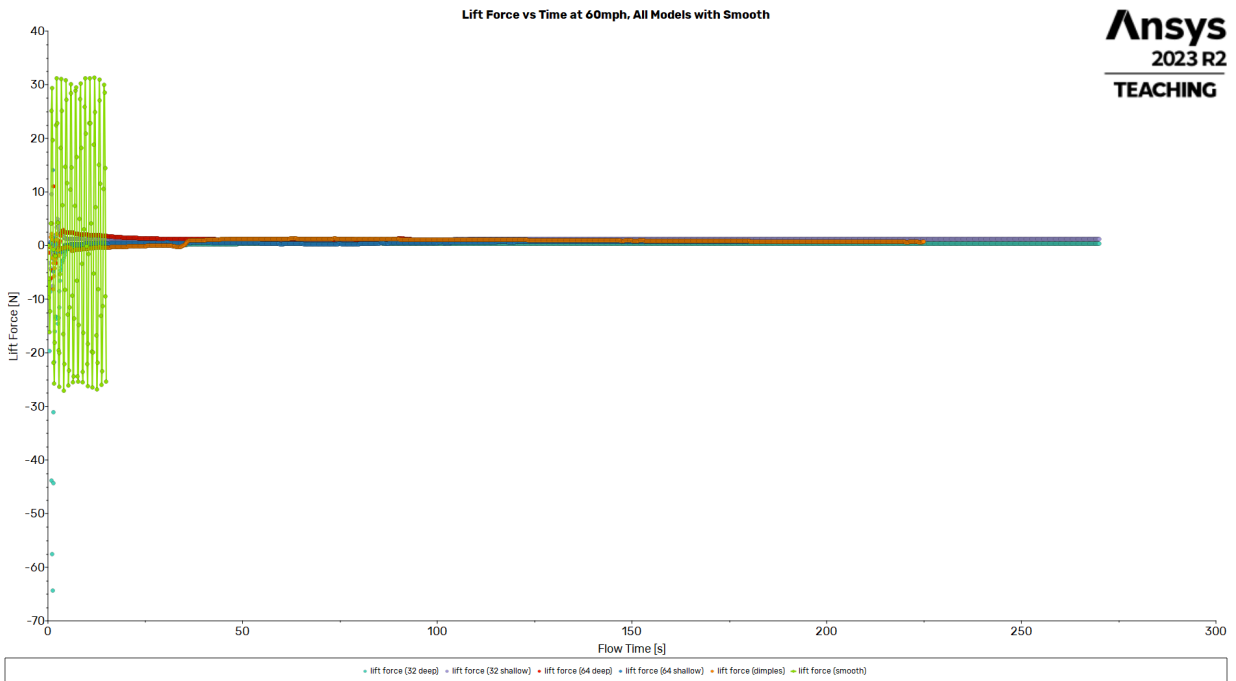
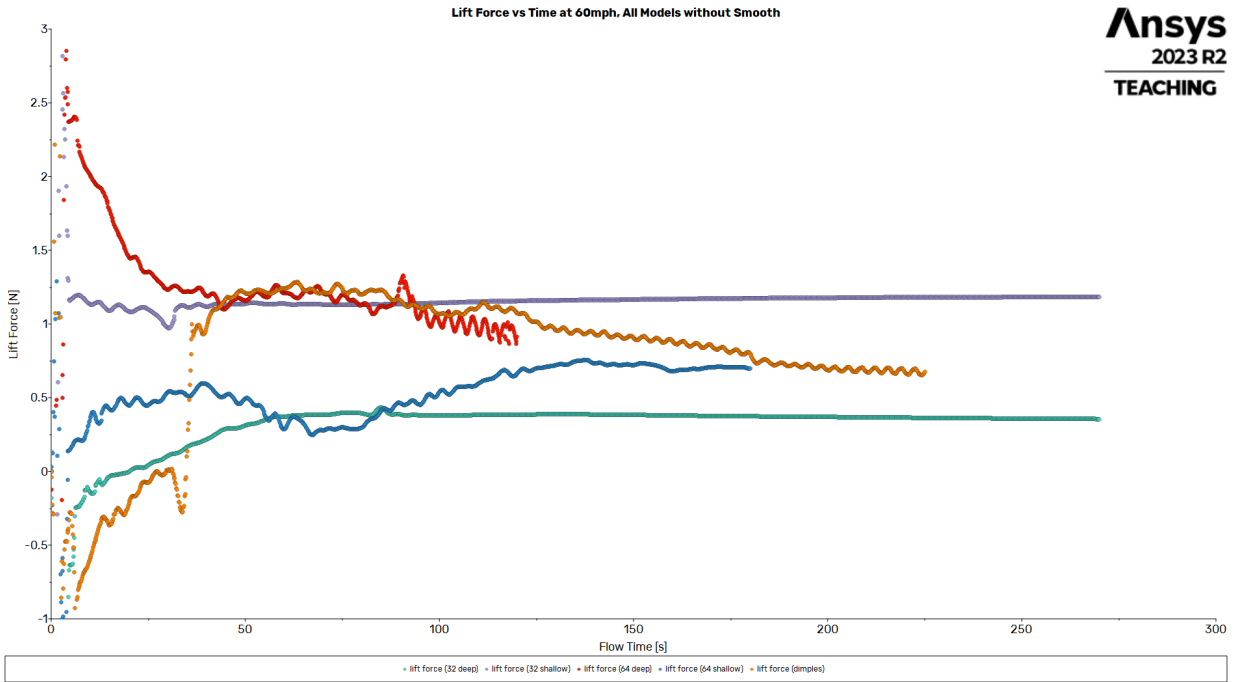
- (1) “The Most Popular Sports in the World.” *WorldAtlas*, 13 Sept. 2023, www.worldatlas.com/articles/what-are-the-most-popular-sports-in-the-world.html.
- (2) “2021 Edition - Img.Mlbstatic.Com.” *OFFICIAL BASEBALL RULES 2021 Edition*, 2021, img.mlbstatic.com/mlb-images/image/upload/mlb/atcjzj9j7wrgvsm8wnjq.pdf.
- (3) “2023 Official Playing Rules of the National Football League.” *2023 OFFICIAL PLAYING RULES OF THE NATIONAL FOOTBALL LEAGUE*, 2023, operations.nfl.com/media/tvglh0mx/2023-rulebook_final.pdf.
- (4) “International Football Association Board.” *Laws of the Game 2021/22*, 2021, downloads.theifab.com/downloads/laws-of-the-game-2021-22?l=en.
- (5) “Jabulani Ball ‘too Perfect’ to Fly Straight - Scientists.” *Phys.Org*, Phys.org, 29 June 2010, phys.org/news/2010-06-jabulani-ball-straight-scientists.html.
- (6) Barber, S., Carré, M. (2009). Soccer Ball Aerodynamics. In: Peters, M. (eds) *Computational Fluid Dynamics for Sport Simulation. Lecture Notes in Computational Science and Engineering*, vol 72. Springer, Berlin, Heidelberg. https://doi.org/10.1007/978-3-642-04466-3_4
- (7) Asai, T., Seo, K., Kobayashi, O. *et al.* Fundamental aerodynamics of the soccer ball. *Sports Eng* 10, 101–109 (2007). <https://doi.org/10.1007/BF02844207>
- (8) Firoz Alam, Harun Chowdhury, Mark Stemmer, Zilong Wang, Jie Yang, Effects of surface structure on soccer ball aerodynamics, *Procedia Engineering*, Volume 34, 2012, Pages 146-151, ISSN 1877-7058, <https://doi.org/10.1016/j.proeng.2012.04.026>. (<https://www.sciencedirect.com/science/article/pii/S1877705812016396>)
- (9) Texier, Baptiste Darbois, et al. “Physics of Knuckleballs - IOPscience.” *IOP Publishing*, 2016, iopscience.iop.org/article/10.1088/1367-2630/18/7/073027.
- (10) Abbas, Zaheer, et al. “Influence of Dimple Design on Aerodynamic Drag of Golf Balls - Researchgate.” *ResearchGate*, 2019, www.researchgate.net/publication/337227398_Influence_of_dimple_design_on_aerodynamic_drag_of_Golf_balls.
- (11) Chowdhury, Harun & Loganathan, Bavin & Wang, Yujie & Mustary, Israt & Alam, Firoz. (2016). A Study of Dimple Characteristics on Golf Ball Drag. *Procedia Engineering*. 147. 87-91. 10.1016/j.proeng.2016.06.194.
- (12) “International Football Association Board.” *Laws of the Game 2021/22*, 2021, downloads.theifab.com/downloads/laws-of-the-game-2021-22?l=en.
- (13) Alam, Firoz & Chowdhury, Harun & Loganathan, Bavin & Mustary, Israt. (2016). A Study of Aerodynamic Drag of Contemporary Footballs. *Procedia Engineering*. 147. 81-86. 10.1016/j.proeng.2016.06.193.

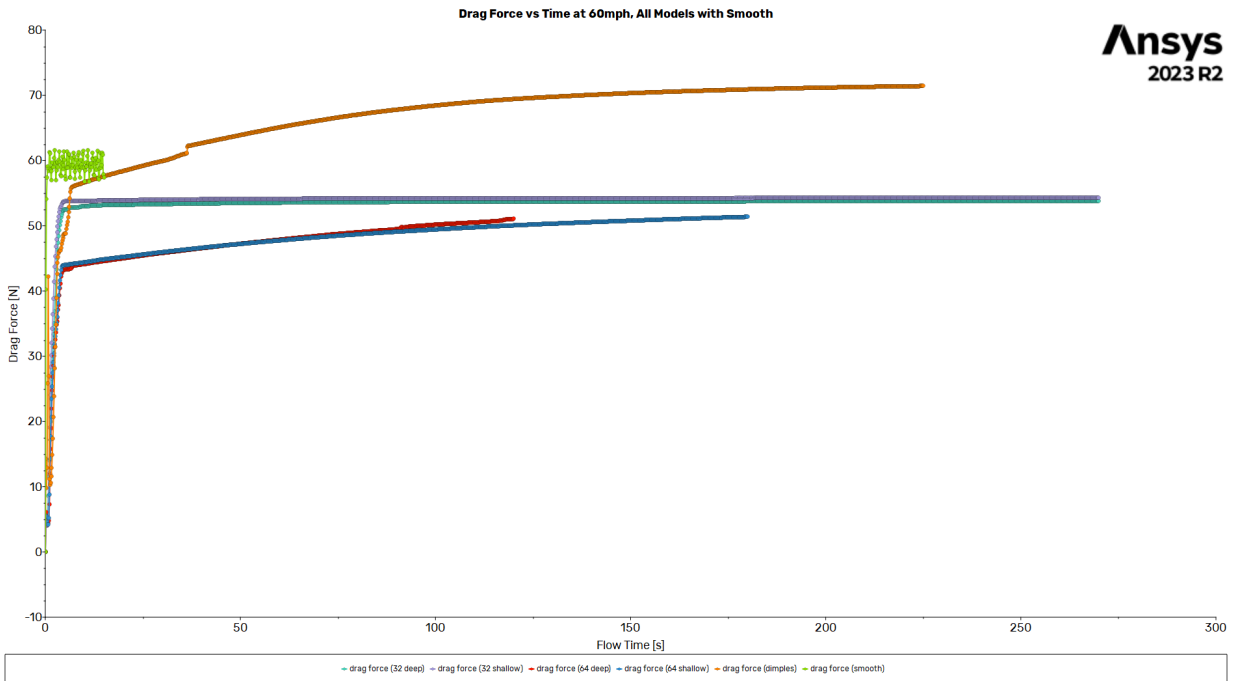
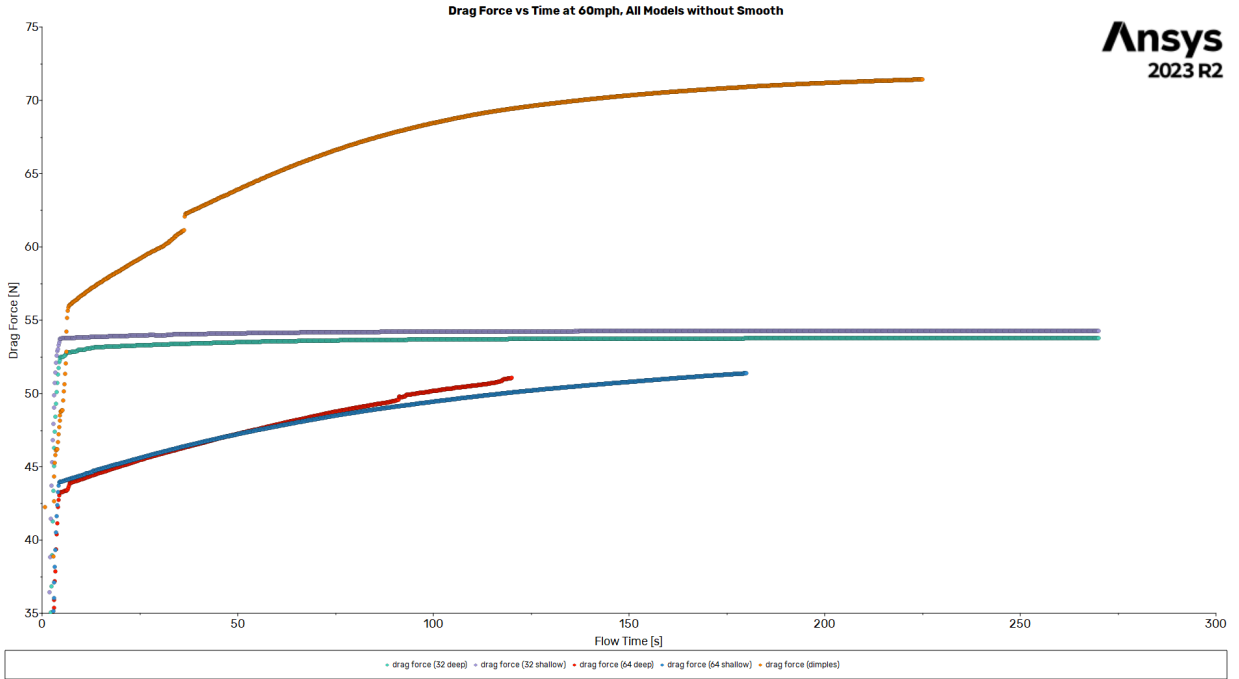
- (14) Goff JE, Hong S, Asai T. Effect of a soccer ball's seam geometry on its aerodynamics and trajectory. *Proceedings of the Institution of Mechanical Engineers, Part P: Journal of Sports Engineering and Technology*. 2020;234(1):19-29. doi:[10.1177/1754337119876485](https://doi.org/10.1177/1754337119876485)
- (15) Goff, John & Hong, Sungchan & Asai, Takeshi. (2018). Aerodynamic and surface comparisons between Telstar 18 and Brazuca. *Proceedings of the Institution of Mechanical Engineers, Part P: Journal of Sports Engineering and Technology*. 232. 175433711877321. 10.1177/1754337118773214.
- (16) Kiratidis, Adrian L, and Derek B Leinweber. "An Aerodynamic Analysis of Recent FIFA World Cup Balls - IOPscience." *IOP Publishing*, 16 Mar. 2018, iopscience.iop.org/article/10.1088/1361-6404/aaa888.
- (17) Fontes, Ed. "Does It Matter Which Ball the FIFA World Cup™ Teams Practiced With?" *COMSOL*, 6 June 2018, www.comsol.com/blogs/does-it-matter-which-ball-the-fifa-world-cup-teams-practiced-with/.
- (18) Hong, S., & Asai, T. (2020). Effect of Surface Groove Structure on the Aerodynamics of Soccer Balls. *Applied Sciences*, 10(17), 5877. MDPI AG. Retrieved from <http://dx.doi.org/10.3390/app10175877>
- (19) Goff JE, Hong S, Asai T. Aerodynamic comparisons between Al Rihla and recent World Cup soccer balls. *Proceedings of the Institution of Mechanical Engineers, Part P: Journal of Sports Engineering and Technology*. 2022;0(0). doi:[10.1177/17543371221140497](https://doi.org/10.1177/17543371221140497)
- (20) Achenbach, E. (1972). Experiments on the flow past spheres at very high Reynolds numbers. *Journal of Fluid Mechanics*, 54(3), 565-575. doi:10.1017/S0022112072000874
- (21) Achenbach, E. (1974). The effects of surface roughness and tunnel blockage on the flow past spheres. *Journal of Fluid Mechanics*, 65(1), 113-125. doi:10.1017/S0022112074001285
- (22) Hong S, Goff JE, Asai T. Effect of a soccer ball's surface texture on its aerodynamics and trajectory. *Proceedings of the Institution of Mechanical Engineers, Part P: Journal of Sports Engineering and Technology*. 2019;233(1):67-74. doi:[10.1177/1754337118794561](https://doi.org/10.1177/1754337118794561)
- (23) Hong, Sungchan & Chung, Chul & Nakayama, Masao & Asai, Takeshi. (2010). Unsteady Aerodynamic Force on a Knuckleball in Soccer. *Procedia Engineering*. 2. 2455-2460. 10.1016/j.proeng.2010.04.015.
- (24) "K-Epsilon Models." *CFD Online*, CFD Online AB, 18 June 2011, www.cfd-online.com/Wiki/K-epsilon_models.
- (25) "18.3.1 Spatial Discretization." *Ansys Fluent 12.0 Theory Guide*, Ansys, Inc., 23 Jan. 2009, www.afs.enea.it/project/neptunius/docs/fluent/html/th/node366.htm.
- (26) Hitti , Natashah. "Nike Ditches Smooth Design for Dimples for Premier League Flight Football." *Dezeen*, 1 July 2020, www.dezeen.com/2020/07/01/nike-flight-ball-premier-league-football-design/.

- (27) Goff, John Eric, and The Conversation US. "Men's World Cup Soccer Ball, the Al Rihla, Has the Aerodynamics of a Champion." *Scientific American*, 20 Feb. 2024, www.scientificamerican.com/article/mens-world-cup-soccer-ball-the-al-rihla-has-the-aerodynamics-of-a-champion/.
- (28) Colen, Jerry. "NASA Turns World Cup into Lesson in Aerodynamics." *NASA*, NASA, 7 Sept. 2023, www.nasa.gov/centers-and-facilities/ames/nasa-turns-world-cup-into-lesson-in-aerodynamics/.
- (29) FIFA. "Al Rihla Following Famous Line of World Cup Balls." *Fifa.Com*, 18 Nov. 2022, www.fifa.com/fifaplus/en/articles/fwc-qatar-2022-world-cup-balls.
- (30) Rice-Coates, Callum. "Adidas Jabulani: The 2010 World Cup's Uncontrollable Ball." *The Independent*, Independent Digital News and Media, 13 June 2020, www.independent.co.uk/sport/football/world-cup/adidas-jabulani-2010-world-cup-ball-south-africa-a9563616.html.
- (31) Ghosh, Pallab. "Engineers Defend World Cup Football amid Criticism." *BBC News*, BBC, 4 June 2010, www.bbc.com/news/10231975.
- (32) Lyjak, Adam. "The Finances behind the 2022 World Cup." *Michigan Journal of Economics*, University of Michigan, 10 Jan. 2023, sites.lsa.umich.edu/mje/2023/01/10/the-finances-behind-the-2022-world-cup/.
- (33) Qatar Moments. "Album: World Cup Match Balls through the Years." *Qatar Moments*, 24 Mar. 2022, www.qatarmoments.com/album-world-cup-match-balls-through-the-years-465279.html#.
- (34) Hosszú, Zoltán. "Made in China Match Ball FIFA World Cup 2010 South Africa Adidas Jabulani." *Www.Worldcupballs.Info*, 2023, www.worldcupballs.info/ball/world-cup-balls/2010-south-africa/made-in-china-match-ball-fifa-world-cup-2010-south-africa-adidas-jabulani/.
- (35) Summerscales, Robert. "Official Al Rihla FIFA World Cup Ball for Qatar 2022 Unveiled by Adidas." *Futbol on FanNation*, Futbol on FanNation, 30 Mar. 2022, www.si.com/fannation/soccer/futbol/news/al-rihla-fifa-world-cup-qatar-2022-ball-unveiled-by-adidas.
- (36) "Nike Unveil the 'flight' Official Match Ball for the 20/21 Season." *SoccerBible*, SoccerBible, 29 June 2020, www.soccerbible.com/performance/football-equipment/2020/06/nike-unveil-the-flight-official-match-ball-for-the-2021-season/.

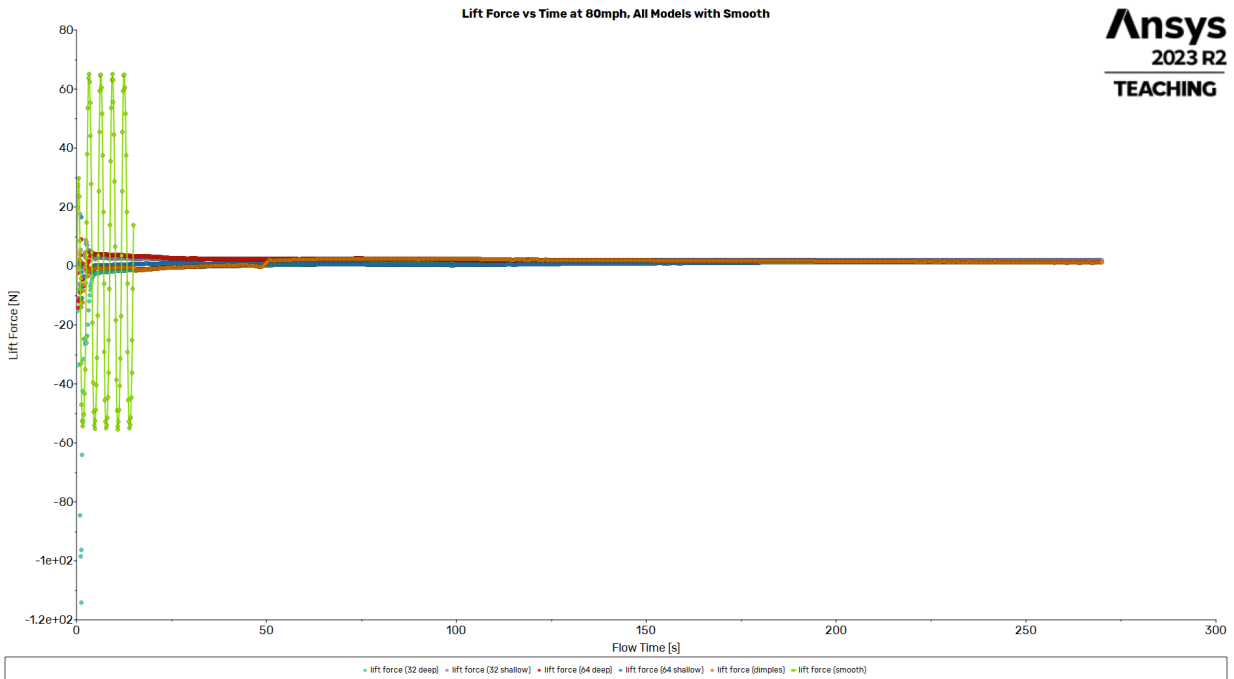
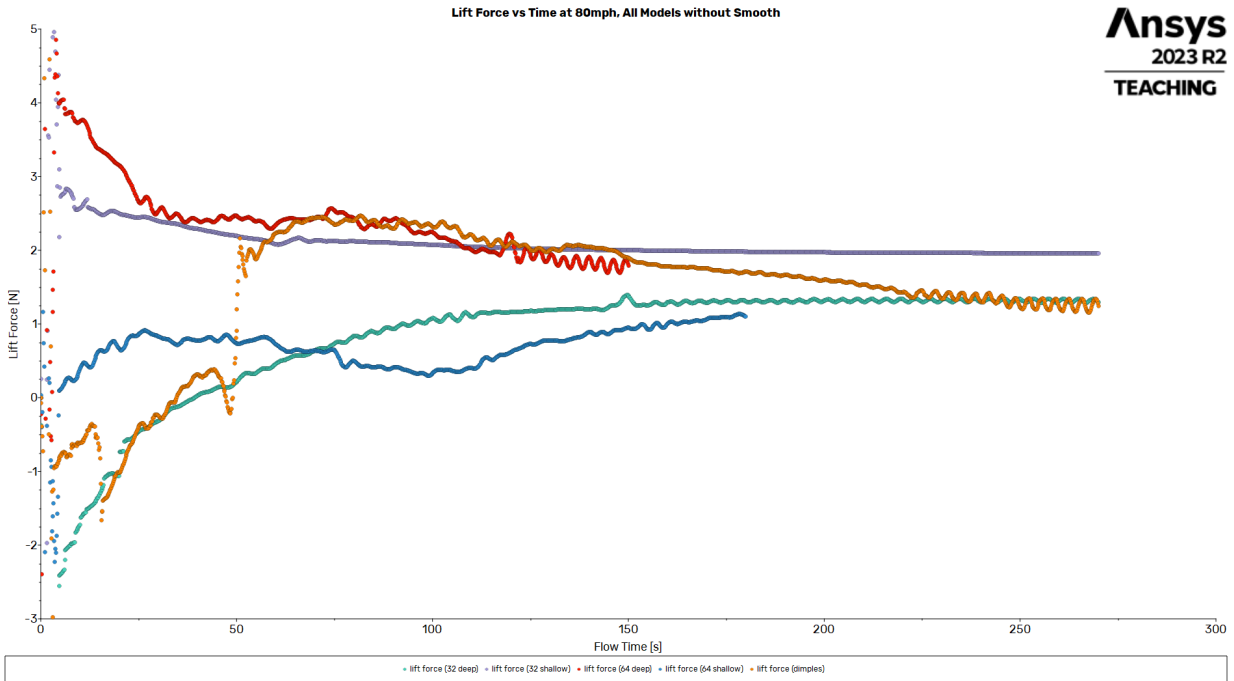
Appendix A: Unscaled Force Graphs

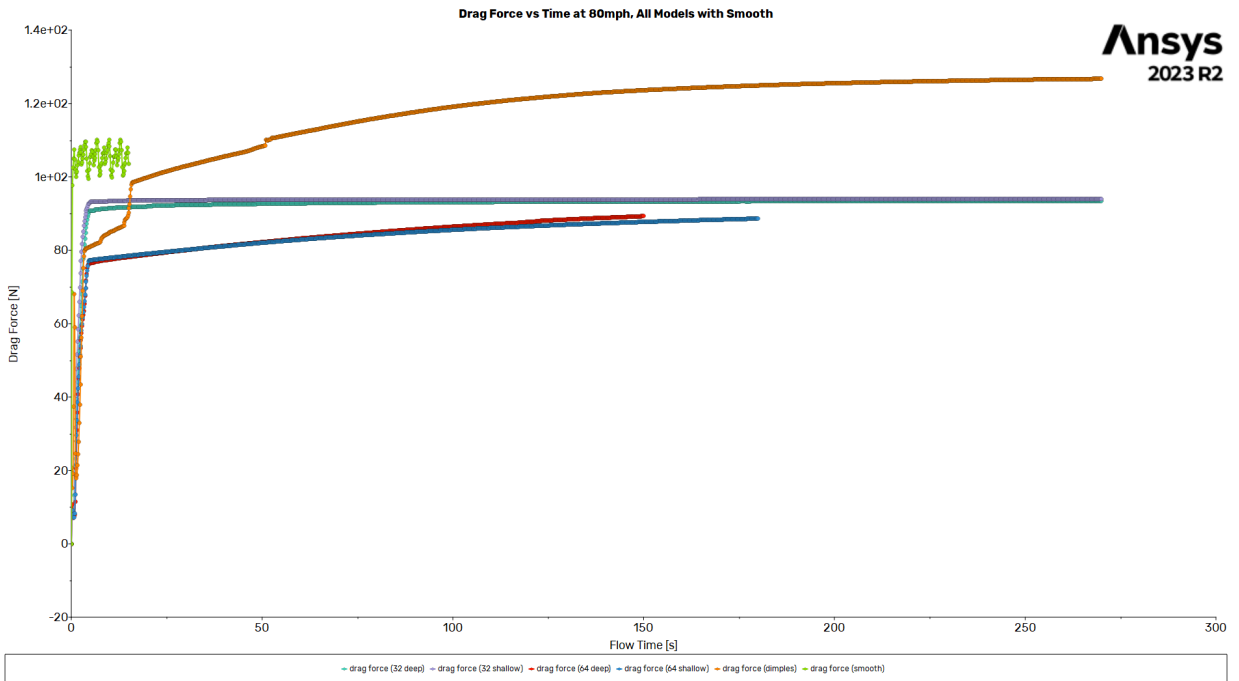
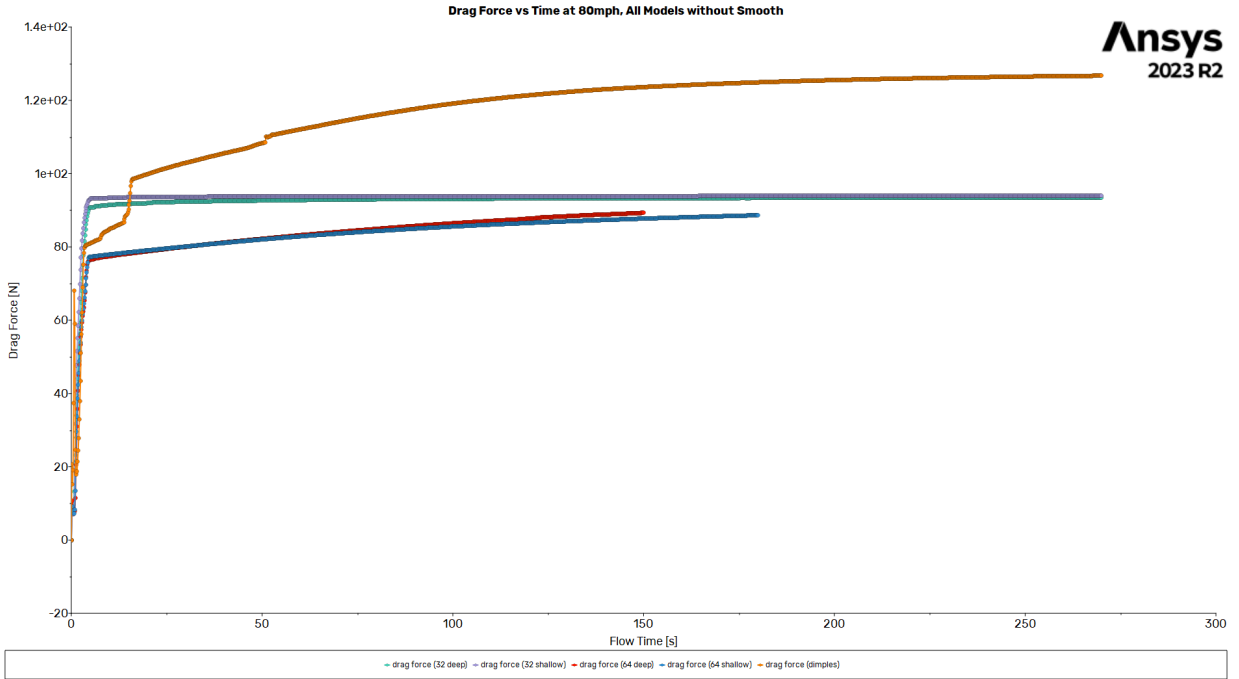
60 mph:





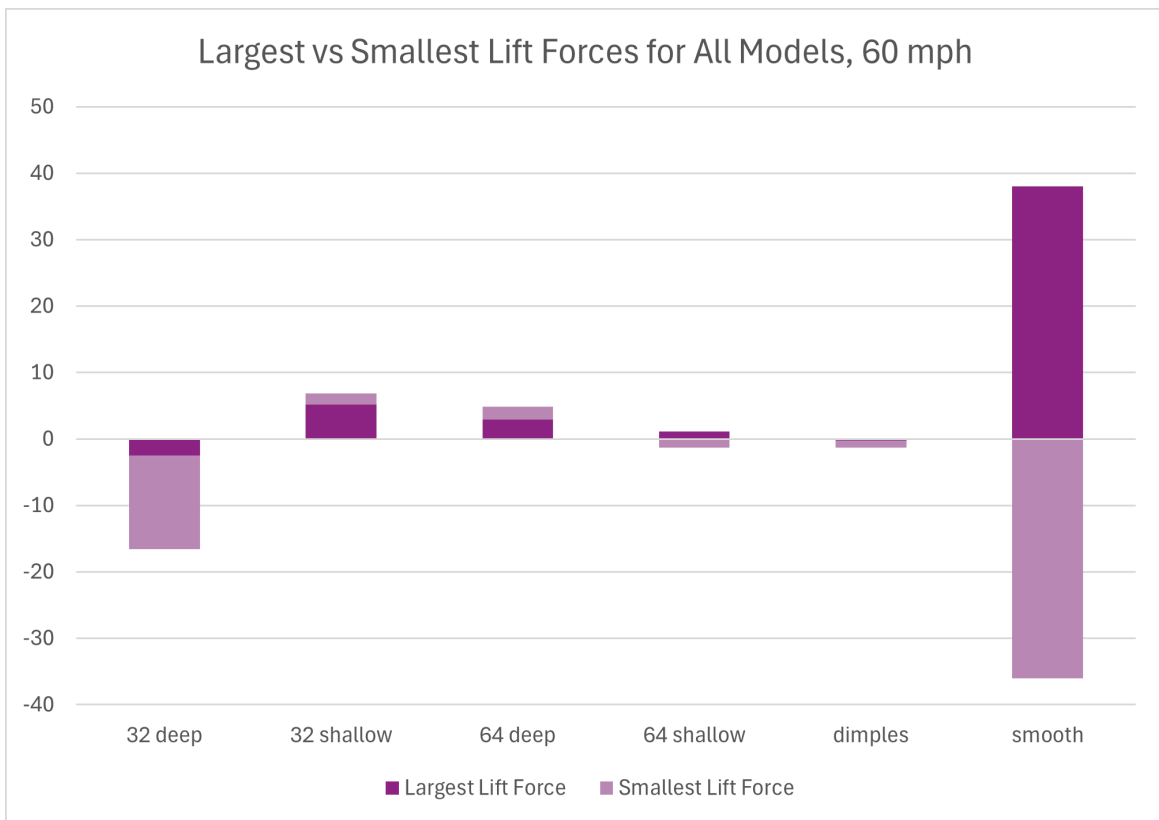
80 mph:





Appendix B: Force Difference Data

60 mph	Largest Lift Force Value (N)	Smallest Lift Force Value (N)	Absolute Difference	Relative Difference to Smooth Ball, Lift Force	Relative Difference from Seam Length (64 vs 32 panel)	Relative Difference from Seam Depth (same panel number, deep vs shallow)
32 deep	-2.47	-14.1	11.63	-84.28%		218.63%
32 shallow	5.24	1.59	3.65	-95.07%		
64 deep	2.95	1.95	1	-98.65%	-91.40%	-59.51%
64 shallow	1.14	-1.33	2.47	-96.66%	-32.33%	
dimples	-0.273	-1.06	0.787	-98.94%		
smooth	38	-36	74	n/a		



80 mph	Largest Lift Force Value (N)	Smallest Lift Force Value (N)	Absolute Difference	Relative Difference to Smooth Ball, Lift Force	Relative Difference from Seam Length (64 vs 32 panel)	Relative Difference from Seam Depth (same panel number, deep vs shallow)
32 deep	-3.84	-28.8	24.96	-81.78%		85.03%
32 shallow	15.7	2.21	13.49	-90.15%		
64 deep	4.91	3.78	1.13	-99.18%	-95.47%	-53.44%
64 shallow	0.227	-2.2	2.427	-98.23%	-82.01%	
dimples	-0.623	-1.19	0.567	-99.59%		
smooth	73	-64	137	n/a		

Largest vs Smallest Lift Forces for All Models, 80 mph

